The Pennsylvanian State University

The Graduate School

THE INFLUENCE OF OBESITY AND ASSOCIATED HYPERGLYCEMIA ON BONE HOMEOSTASIS

A Thesis in

Anatomy

by

Jared T. Michaels

Submitted in Partial Fulfillment
of the Requirements
for the Degree of

Master of Science

May 2021

The thesis of Jared T. Michaels was reviewed and approved by the following:

Reyad Elbarbary
Assistant Professor of Orthopaedics and Rehabilitation
Thesis Advisor

Patricia McLaughlin
Professor of Neural and Behavioral Sciences
Director of Anatomy Graduate Program

Fadia Kamal
Assistant Professor of Orthopaedics and Rehabilitation

Gregory Lewis
Assistant Professor of Orthopaedics and Rehabilitation

ABSTRACT

Obesity is a world-wide disorder that can lead to further metabolic diseases. Hyperglycemia can result from a prolonged state of obesity, which when combined with developed insulin resistance can lead to metabolic disorders like Type 2 Diabetes Mellitus (T2DM). Of the body's various responses to metabolic disorders, chronic inflammation is one that is well-known. The prolonged state of inflammation has been found to impact the health of bone. Further investigation into the mechanism, which connected obesity to the bone health, was required. We applied various techniques to evaluate the bone secondary structure and microstructure between Diet-Induced Obesity (DIO) mice and lean mice. Micro-computed tomography (μCT) of the tibia and femur indicated that obesity negatively impacted the trabecular bone. Bone volume (BV/TV), trabecular number (Tb.N), and bone mineral density (BMD) were found to be decreased in DIO samples when compared to the lean samples. The trabecular separation (Tb.Sp) was inversely related to the decrease in Tb.N for both the tibia and femur. Interestingly, there were undetectable differences in the cortical tibia between lean and DIO mice. Second harmonic generation (SHG) microscopy provided analysis of the collagen microstructure of the cortical bone. DIO mice were found to have elevated immature collagen fibers as well as accelerated collagen fiber disorganization. Obesity resulted in changes to the collagen microstructure that were not detectable in the cortical secondary structure by 8-months of age.

Proteomic analysis of complete bone samples provided information that a proteoglycan, lumican, was one of the proteins to be substantially elevated in 5-month-old DIO mice. This finding guided further exploration into the role that lumican has throughout the extracellular matrix (ECM) of obese mice. Immunofluorescent (IF) staining confirmed that there was more

lumican positive areas in DIO mice. We found the presence of lumican to be significantly elevated in the bone marrow of DIO mice. Quantitative polymerase chain reaction (qPCR) of both trabecular bone tissue and isolated bone marrow confirmed that lumican was being expressed in higher quantities in DIO samples. The function of lumican in the bone marrow was further evaluated. To determine if lumican was associated with cellular apoptosis in obese mice, a TUNEL stain was performed. After confirming that DIO samples had elevated apoptosis, serial sections were used to compare regions of lumican expression to areas with higher apoptosis. This finding indicated that lumican may have a degradative effect in the bone marrow ECM. For further confirmation of lumican's role, we had to determine which cells expressed lumican.

Fluorescent-Activated Cell Sorting (FACS) allowed for the isolation of stromal cells from mouse bone marrow. By comparing stromal cells to hematopoietic cells, we found via qPCR that stromal cells express lumican. To begin to isolate which cells of the stromal fraction expression lumican, IF-staining was used. A co-staining method was developed to detect any co-localization between Stem cell antigen-1 (Sca-1) and Lumican. The Sca-1 is a selective marker to identify mesenchymal stem cells (MSCs). All areas of lumican expression were co-localized with Sca-1 signals, while not all Sca-1 signal co-localized with lumican signals. This experiment will need further verification by increasing the sample size.

Bone homeostasis in DIO mice was found to be altered. It was also discovered that elevated lumican expression was associated with increased apoptosis in the bone marrow of DIO mice. Further determination of the connection between Lumican and MSCs requires *in vitro* cellular experiments. By determining which cells express lumican in DIO samples, we can explore the association between lumican and apoptosis in the bone marrow.

TABLE OF CONTENTS

List of Figures

Chapter 2

Chapter 3

Chapter 4:

LIST OF TABLES

ACKNOWLEDGEMENTS

I would like to start by thanking Dr. Reyad Elbarbary for allowing me to gain research experience as a member of his team. Having the opportunity to further my scientific skills over the past year has given me a greater appreciation for basic and translational science. When I started in Dr. Elbarbary's lab, I had little experience with various lab techniques. I am grateful that I was able to learn about surgical techniques, histological sectioning, immunofluorescent staining, and numerous others. I would like to also extend my appreciation towards the other members of the lab: Deepak, Irena, and Marwa. They provided countless support throughout experiments and trained me in the lab techniques that I described. I would also like to thank my thesis committee for their support and advice throughout this process. Dr. Patricia McLaughlin, Dr. Fadia Kamal, and Dr. Greg Lewis provided encouragement and expertise on aspects of my project for which I am grateful. Members of Dr. Kamal's lab: Venga, Gina, Bill, and Natalie, were also crucial towards my growth as a scientist as they were readily available to help me in times of confusion. The Center for Orthopaedics Research and Translational Science provided me with a welcoming atmosphere to learn and conduct research in a field of my interest.

I would also like to thank my wife, Kezia, for her unending support and confidence in me. She was always willing to go above and beyond for me throughout our years together so that I can continue my academic path. As I continue to pursue a career in medicine, she constantly gives me words of encouragement and help me decompress from the rigors of my studies. She is willing to help me in any way possible as to ensure that I can achieve my goals and for that I am forever grateful.

My family and friends have always been a support system for me. Whether it is from medically related discussions with my parents, or simply talking about sports with my brother, I

can feel their love. They have and continue to encourage me to achieve my dreams of becoming a physician. I am always appreciative of being able to step away from my studies for a brief time to relax and spend quality time with them. My friends have always encouraged me to succeed. They may not be able to directly relate to my area of academics, but they know how to support me. Whether we are playing videogames, spending time in nature, or having game nights are all ways that we can forget about the real world for a brief moment. Having endless resources through my family and friends allow me to confidently become the person I want to be. I cannot wait to share my future success with them to show my thanks for all their support.

The funding for the research in this project was supported by the National Institutes of Health (NIH) RO1 DK121327-01A1. Any opinions, findings, and conclusions or recommendations expressed in this publication are those of the author and do not necessarily reflect the views of the NIH.

There is nothing to disclose.

Chapter 1: Introduction

Obesity's influence on bone microstructure

Throughout the world population, roughly one third of people are classified as either overweight or obese. In young adults, men had a higher prevalence of being overweight than women. After age 45, women are generally more susceptible to obesity than men; mostly due to menopausal side-effects.(1) Obesity is a major factor that can influence bone health as well as lead to metabolic diseases. One metabolic disorder is Type-2 diabetes mellitus (T2DM). This form of diabetes mellitus (DM) is associated with hyperglycemia and insulin resistance.(2) Hyperglycemia can result from increased blood glucose levels from glycogenolysis and gluconeogenesis from the liver and lack of glucose uptake from muscle.(2) By 2030, it was projected that 366 million people in the world would have obesity-induced diabetes.(2, 3)

Glucose homeostasis is a key factor in DM and is primarily regulated by insulin. The primary functions of insulin are to allow fat deposition in adipocytes, trigger an influx of glucose into muscle, and stimulate glycogen synthesis.(2) One minor role of insulin is to aid in an anti-inflammatory response.(2) Inflammation can result when hyperglycemia impedes proper insulin function.(2) Chronic inflammation has been associated with prolonged elevated levels of proinflammatory cytokines.(2, 4, 5) Tumor necrosis factor-α (TNF-α), Interleukin-1β (IL-1β), and Interleukin-6 (IL-6) are the proinflammatory cytokines found at increased levels in adipose tissue.(2, 4-7) The adipose tissue in relation to obesity is found to have elevated levels of macrophages that produce inflammatory cytokines.(4) Adipocytes can undergo apoptosis in response to insulin insensitivity. The site of apoptosis with result with an influx of macrophages that lead to inflammation.(2) Obesity has been found to cause adipose tissue to develop in the bone marrow. The elevated expression of receptor activator of nuclear factor kappa-B ligand

(RANKL) has been found as a result of increased marrow adiposity.(8) Bone resorption is associated with osteoclast differentiation by inflammatory cytokines stimulating the RANK/RANKL/OPG pathway.(4) RANKL is a signaling molecule that will bind to RANK receptor to mediate the advancement of the developing osteoclast.(9) Osteoprotegerin (OPG) is released from osteoblasts to interfere with RANK-RANKL binding, thus preventing osteoclast development.(9) The proinflammatory cytokines will increase osteoclastogensis by increasing the frequency that RANKL binds to RANK.(4, 9) The increase in these cytokines and macrophages will result in an increase in osteoclast activity.(6, 7)

There is another mechanism that utilizes the RANKL pathway for bone remodeling. Parathyroid Hormone (PTH), which is secreted from the parathyroid glands, regulates the influence of calcium on the bone and kidneys.(10) Within the bone, PTH will regulate the release of calcium to the ECM as a result of bone turnover. As a major regulator in bone remodeling, PTH can bind to its receptor on the osteoblasts. When bound, this will indirectly allow the activation of the osteoclast for bone resorption.(10) The elevated levels of PTH also leads to an increase of RANKL. The actions of PTH is believed to be one of the reasons for a decrease in bone mineral density for people with hyperthyroidism.(10)

Another mechanism to influence bone health involves the formation and fate of osteoblasts. Mesenchymal Stem Cells (MSCs) serve as the precursor for both osteoblasts and adipocytes.(5, 11) For the development of osteoblasts, the peroxisome proliferator-activated receptor gamma (PPAR-γ) and WNT signaling pathways are utilized. The Wnt signaling pathway activates the initiation of osteogenesis and prevention of adipogenesis.(5, 11) If the PPAR-γ pathway is exposed to reactive oxygen species, then the adipocytes will develop from MSCs. Hyperglycemia has been found to increase sclerostin; a protein that will inhibit the Wnt

pathway in bone marrow MSCs.(5, 11) The interaction of sclerostin and Wnt has been found to lead to increased marrow adipose tissue.(8)

Many believed that an increase in body mass would result in an increase in BMD.(6) It turns out that obesity has a negative correlation with osteoblastogenesis resulting from marrow adipogenesis.(6) With a high fat diet, an increase in osteoclast formation from bone marrow cells is associated with an increase in serum TRAP.(6) Serum TRAP is a bone resorption marker that can be found on osteoclast-like cells.(6) Another mechanism of bone metabolism is from influence of an increase in adipogenesis with a decrease in osteoblastogenesis. This is a possibility as both osteoblasts and adipocytes are products of a similar mesenchymal stem cell (MSCs) pathway.(6, 12) The differentiation between the two cell lines is a result of differing transcription factors.(12) It has been found that postmenopausal, osteoporotic patients have MSCs that express more adipocyte-related markers from within the bone-marrow.(12)

Human micro-computed tomography (μCT) bone measurement trends

In humans, an increase in fatty tissue has identified as a potential risk factor for a decrease in bone mineral density (BMD) when associated with other metabolic diseases.(12) Obesity was generally believed to have a protective effect on bone.(12) More recently, it has been suggested that prolonged obesity can lead to osteoporosis in men and women, which is known to decrease BMD.(12) In other studies, postmenopausal women with obesity were found to have an increase in trabecular number (Tb.N) with a decrease in trabecular separation (Tb.Sp) and trabecular thickness (Tb.Th) in adults.(13, 14) These changes in microstructure were associated with an increase in the volume of BMD.(13, 14) For the cortical bone, there was an increase in cortical thickness (Ct.Th).(13, 14) Little has been published regarding obesity alone to clarify the exact mechanism obesity has on bone.

Obese animal models

Of the many obesity animal models, there are two popular animal models that correlate to T2DM. One mouse model is the result of a leptin deficiency. The monogenic, leptin-deficient mice present with T2DM by being obese with mild hyperglycemia.(15, 16) Leptin's physiological pathway in mice is to bind to the leptin receptor in the brain within the hypothalamus. When leptin binds to its receptor, it will signal a JAK-STAT3 pathway to suppress orexigenic peptides and increase anorexigenic peptides.(17) Orexigenic peptides will generally increase food consumption, while anorexigenic peptides decrease food consumption. Mice that have low leptin levels have been found to have increased orexigenic peptides and a decrease of anorexigenic peptides.(17) In leptin-associated obesity, there are two mechanisms that may result in lack of signaling: there could be a nonfunctional leptin receptor, or a inhibition of leptin protein. One inhibitor of leptin, SOCS3, prevents the transport of leptin across the blood-brain-barrier within the hypothalamus.(17) This prevents leptin from binding to the leptin receptor, which maintain elevated leptin levels and the inability to suppress orexigenic peptides.(17) The leptin deficient mouse model is less commonly representative of the pathogenesis to obesity in humans.(16) The polygenic model, the DIO mouse model, more accurately represents obesity in humans. The state of obesity is reached in a similar manner when compared to humans.(16, 18) Specifically, the C57BL/6J strain is prone to obesity with hyperglycemia, hyperinsulinemia, and weight gain from a consumption of excess calories.(16, 18). These mice were found to develop these pathologies when fed a high fat diet *ad libitum* when compared to mice on a normal chow diet.(18) The DIO mice that developed pathologies similar to that observed in obese humans were better representative of the health condition we were exploring.

Trabecular and cortical bone has been found to be influenced by obesity in mice. Microcomputed tomography has been utilized for the detection of the influences to the bone structure in obese mice. Trabecular bone volume ratio was found to be decreased in diet-induced-obesity (DIO) models of C57BL/J6 mice when compared to regular diet mice.(6, 7) Diet induced obesity has also been found to increase Tb.Sp and decrease Tb.N, Cr.Th., and bone area.(6, 7, 19, 20) There has even been evidence of a greater decrease in bone volume ratio with an increase in the duration of high fat diet (HFD).(7, 21, 22) Obesity in mice has been shown to negatively correlate with bone mass when paired with HFD.(7, 21, 22) Some studies have found that cortical bone has been found not to have significant changes in relation to obesity. The bone area and cortical thickness has been indicated to have insignificant changes in the femur.(6, 22) It has been found that HFD didn't have significant change in cortical bone of the tibia regarding Ct.Th and bone area.(21) Another study found that there was no significant impact of HFD on cortical bone until 12 weeks of age.(20) As the μCT can be limited for quantitation of the bone secondary structure, second harmonic generation (SHG) can allow for the detection of changes at the collagen level.

SHG and collagen fibers

The change of bone structure throughout aging could result from natural depletion of collagen I (Col I) fibers. The collagen is also able to be depleted due to being damaged from advanced glycation end products (AGEs).(23) Within proteins, reducing sugars can form covalent bonds with free amino groups.(24, 25) The development of AGEs are a result of non-enzymatic glycation. The Maillard reaction can lead to the development of glucose-mediated intermolecular cross-links within post-translational modified proteins.(24) The cross-link density of collagen fibers will change resulting in more stiff cortical bone.(25) AGEs accumulation are

suggested to increase the osteoclast resorption activity by being correlated with larger and more resorption pits.(24)

SHG microscopy is a prominent method to quantitatively analyze fibrillar collagen organization.(26-28) SHG is a non-linear optical process, in which two photons of the incident light combine to generate a single photon with double the energy (doubling the frequency) and half the wave length.(26-28) SHG can be used only for specific types of proteins that are without a center of symmetry, with fibrillar collagen being the most studied.(26-28) SHG is able to utilize a label-free technique, while remaining sensitive to changes that occur in fiber organization under different conditions such as disease states.(26-28) SHG will provide structural information about collagen-fiber orientation (orientation index), geometry (fiber diameter), and cross-link density.(28) Forward Second Harmonic Generation (FSHG) corresponds to the emitted signal matching the same direction as the excitation signal. Generally if mature collagen is used as the medium, between 80% and 90% of the emission will be in the forward direction.(26, 27) The immature collagen fibrils' emission will typically be in the backwards direction; giving a Backwards Second Harmonic Generation (BSHG).(27) Through the usage of SHG, we were able to observe the collagen-fiber orientation index (OI), collagen-fiber diameter (FD), and collagen cross-link density.

Lumican acts as a signaling molecule in the ECM

Lumican is an extracellular matrix protein that is considered to be a small, leucine rich proteoglycan (SLRPs).(29) It was first characterized in the cornea of a chick as a corneal keratan sulfate proteoglycan.(30) Lumican was initially identified to have a role in corneal transparency. More recently, lumican has been detected in various tissues: mouse cornea, bovine keratocytes, bovine aorta, and even in human kidney, lung, and articular cartilage.(30) The expression of

lumican has been found in interstitial connective mesenchymal cells of adult animals and developing embryos.(31) The detection of mRNA for lumican has also been reported to vary in levels throughout numerous organ systems with the heart and cornea having the highest levels of expression.(31) One role of lumican corresponds with the interaction of keratocan in cornea stroma. When lumican and keratocan are removed, the collagen fibril diameter and spacing are altered, indicating a regulation role in ECM assembly.(29, 31) Lumican can induce intracellular signaling from certain amino acid sequences binding to cell surface receptors. This can lead to apoptosis, cell proliferation, and differentiation.(29) A lack of lumican has been found to cause skin fragility in mice.(29, 31) Lumican has been found to play a role in wound healing depending on the glycation state. The proteoglycan has also been associated with some metastasis as well as tumorigenesis in different types of cancer.(29)

Chapter 2: Effect of Obesity on Bone Structure

To study the influence of obesity on bone health, DIO mice were purchased. The C57BL/6J strain of mice are known for their susceptible nature of obesity. We expect that obesity will negatively impact the bone secondary structure and strength in mice.

DIO animal model

Male 5-month and 8-month-old C57BL/6J mice, stock number 000664, were purchased from the Jackson Laboratory (Bar Harbour, ME, USA). DIO male C57BL/6J mice, stock number 380050, were also purchased from Jackson Laboratory of the same age groups. Mice were housed at a 12-h light/dark cycle, temperature conditions ranging from 21.1-22.8ºC, and 30-70% humidity. During a two-week incubation period, the mice were given their respective diets. The lean diet consisted of 10 kcal % fat, while the high fat diet (HFD) was 60 kcal % fat (OpenSource Diets, Research Diets Inc.). Each group maintained their respective diets until time of sacrifice. For hyperglycemic verification, mice were fasted for six hours followed by measuring fasting blood glucose level using One Touch Ultra (Lifescan). Following anesthetization by use of 5% isoflurane, blood was drawn from the tail vein for measurement. All animal protocols were approved by the Institutional Animal Care and Use Committee (IACUC) of the Pennsylvania State University College of Medicine.

Glucose Tolerance Test was done to observe the efficiency of glucose metabolism. The mice were injected via IP with 2g/kg of glucose following a 6-hour, daytime fast. The time interval for measurements were 15, 30, 60, 90, and 120 minutes.

Tibia and femur harvest from the mice

Mice were sacrificed and the hind limbs were detached just distal to the femoral neck. Following removal of the soft tissues from the bone, a surgical blade was used to detach both the

distal and proximal epiphyseal plates to expose the marrow cavity. Samples were preserved as whole limbs in formalin and then paraffin embedded.

DIO mice had increased total fat percentage and body weight

Body weight was measured using a dual energy x-ray absorptiometry (DEXA). On average, the DIO groups had an increased average total fat percentage and average body weight than the respective lean group. When comparing the two groups, the DIO mice had significantly increased body fat percentage (Figure 2.1: A).

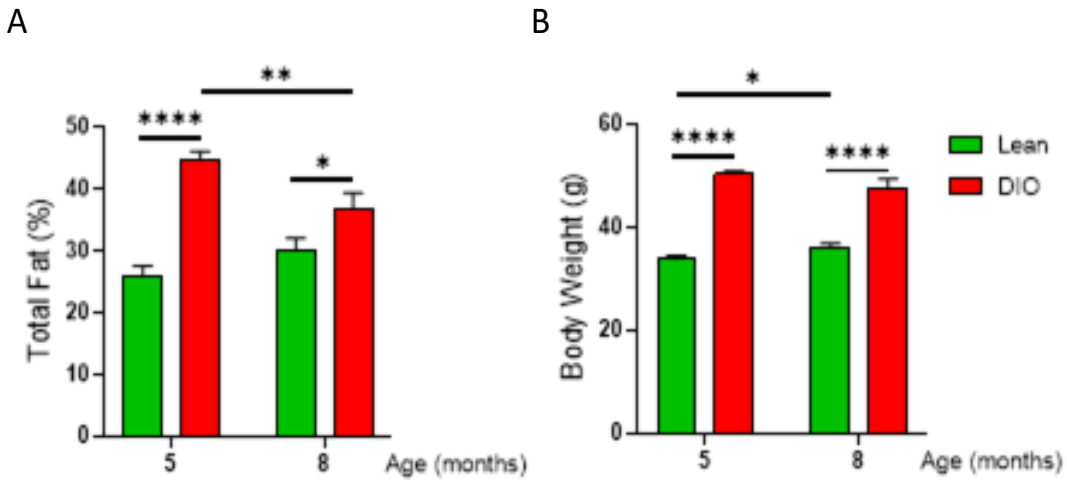

Figure 2.1: Differences in average total fat percentage (A) and average body weight (B). Results are expressed as mean with +/- SEM, $p < 0.05$ (*), $p < 0.01$ (**), $p < 0.001$ (***), $p < 0.0001$ (****), n=11 or 12.

There was a significant increase in body weight for the DIO mice for each age group. (Figure 2.1: B). The difference in body weight for between the DIO and lean mice indicate that the samples reached an obese state.

Blood glucose levels were elevated in DIO mice

Glucose Tolerance Test confirmed hyperglycemia. Fasting Blood Glucose levels were taken and then averaged together. The blood glucose levels were measured at 15 minutes, 30 minutes and then 30-minute intervals for a total time of 120 minutes. Over the total time, the

DIO mice had significantly elevated average blood glucose level when compared to the lean group (Figure 2.2).

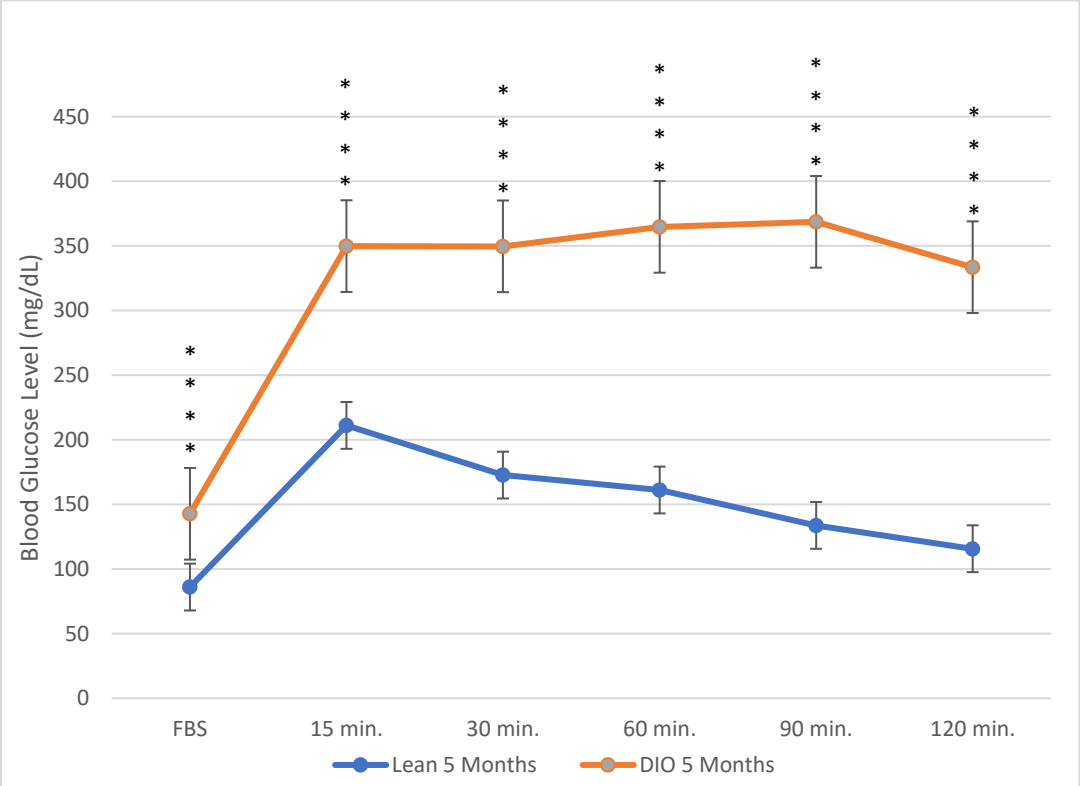

Figure 2.2: Determination of obesity by glucose tolerance test by measuring blood glucose over 120 minutes. Results are expressed as mean with +/- SEM, $p < 0.0001$ (****), n=12

The hyperglycemic state was achieved by the age of 5-months. Elevated blood glucose levels indicate that the DIO mice had become insensitive to insulin.

Trabecular bone features are altered by obesity as determined by µCT

µCT allows for the visualization of bone mineral distribution and analysis of trabecular and cortical bone secondary structures. Generally, mouse trabeculae can be observed at a voxel size of 5-60 µm.(32, 33) Commonly, 9-18 µm is used for analysis of bone microstructure in mice.(6, 7, 19, 20, 32-34)

µCT scanning was done on a Scanco vivaCT 40 for assessment of the distal metaphysis of the femur, scanning was performed using a 10.5µm voxel size at 55kVp, 145mA, and integration time of 300ms. The entire lower extremity of the mice was scanned in succession

beginning at the proximal metaphysis of the femur to the distal aspect of the tibia-fibula junction. Gray scaled, cross-sectional slices with a standard Gaussian filter were applied while being segmented by a constant threshold of 250. Manual contouring of the volume-of-interest for trabecular bone of the femur started proximal to the distal epiphyseal plate and 70 slices were analyzed in the proximal direction. Scanco scripts were used to evaluate Tb.Th, Tb.N, Tb.Sp, BMD, bone volume to total volume ratio (BV/TV) and connectivity density (Conn.D) (Scanco Medical). The same procedure was applied to analyze trabecular tibia with the exception that manual contouring was in the distal direction beginning at the proximal epiphyseal plate. For cortical tibia, the mid-diaphysis region was analyzed. Manual contouring occurred over the distance of 95 slices, starting at 415 slices distal to the proximal epiphyseal plate. Scanco scripts were used for analysis of cortical bone area, Ct.Th, cortical area fraction (BA/TA), and BMD (Scanco Medical). Statistical analysis for the results was done using student's t-test.

Similar results were obtained between the trabecular bone in the femur and tibia. For the trabecular femur, the BV/TV was significantly higher in the lean group of 5 months compared to the DIO group of 5 months. The BV/TV of 5-month-old lean group was significantly higher than the 8-month-old lean group. The BV/TV of the 8-month-old lean group was significantly higher than the 8-month-old DIO group (Figure 2.3: B).

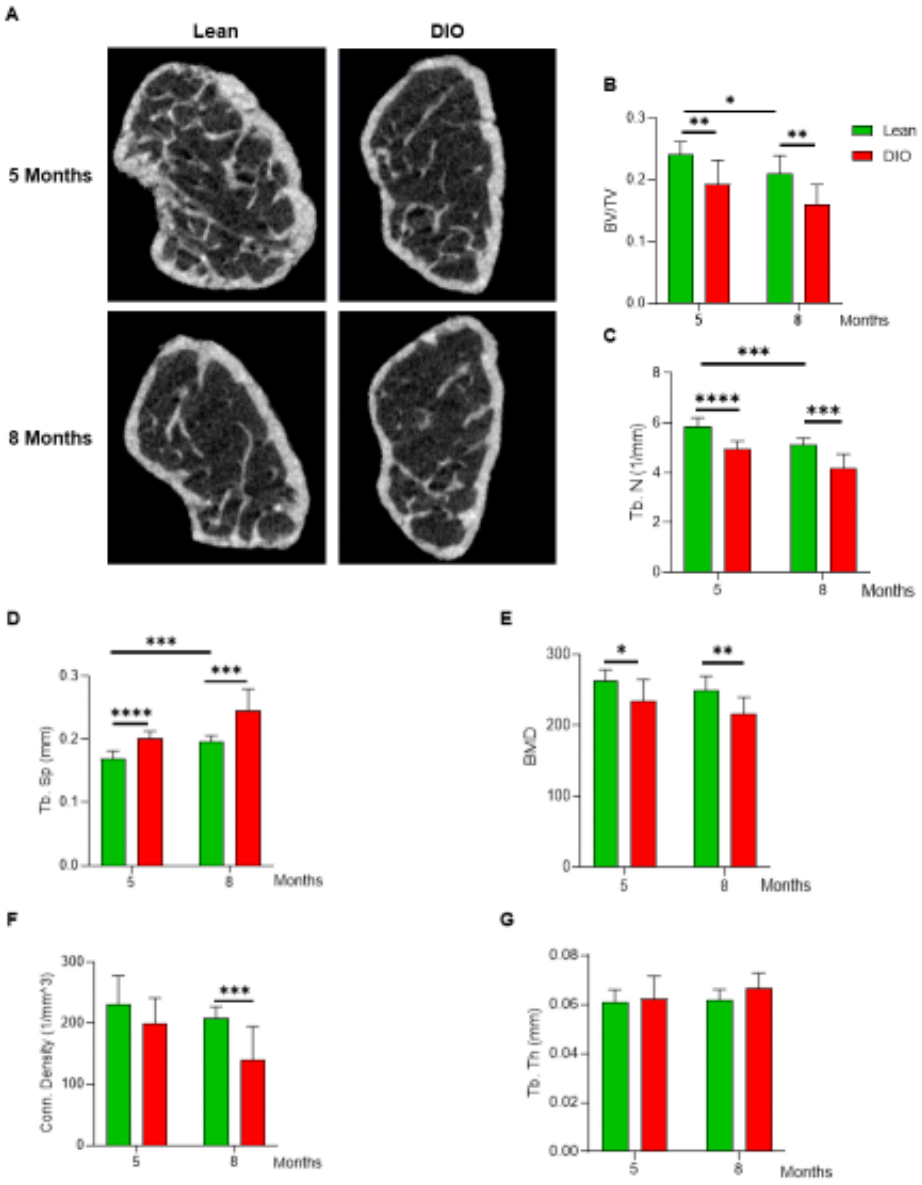

Figure 2.3: µCT analysis of the trabecular femur. (A) µCT images of the trabecular femur. (B-G) Analysis of µCT parameters from the trabecular femur. Results are expressed as mean with +/- SEM, $p < 0.05$ (*), $p < 0.01$ (**), $p < 0.001$ (***), $p < 0.0001$ (****), n=8 or 9.

The trabecular number (Tb.N) of 5-month-old lean group was significantly higher than the 5-month-old DIO group. The Tb.N of the 8-month-old lean group was significantly higher than the 8-month-old DIO group. The Tb.N of the 5-month-old lean group was significantly higher than the 8-month-old lean group (Figure 2.3: C). The trabecular separation (Tb.Sp) was inversely related to the Tb.N. The Tb.Sp of 8-month-old DIO group was significantly higher than the 8-

month-old lean group. Between the 5-month old groups, the DIO had a significantly higher Tb.Sp than the lean group. Within the two lean groups, the 8-month-old group was significantly higher than the 5-month-old group (Figure 2.3: D). The bone mineral density (BMD) was significantly higher in lean samples when compared to DIO within the age groups for the femur (Figure 2.3: E). The Conn.D was significantly higher in the 8-month-old lean group compared to the 8-month-old DIO group (Figure 2.3: F). There was no statistical significance between diet groups or age groups for trabecular thickness (Tb.Th) (Figure 2.3: G).

The trabecular bone in the tibia had similar results as in the femur. There were significant differences for the Tb.N and Tb.Sp that followed the pattern displayed for the respective measurements of the trabecular femur. There One of the differing results was in the BV/TV as the only significance decrease of ratio was between the 5-month-old lean and 8-month-old DIO mice (Figure 2.4: A).

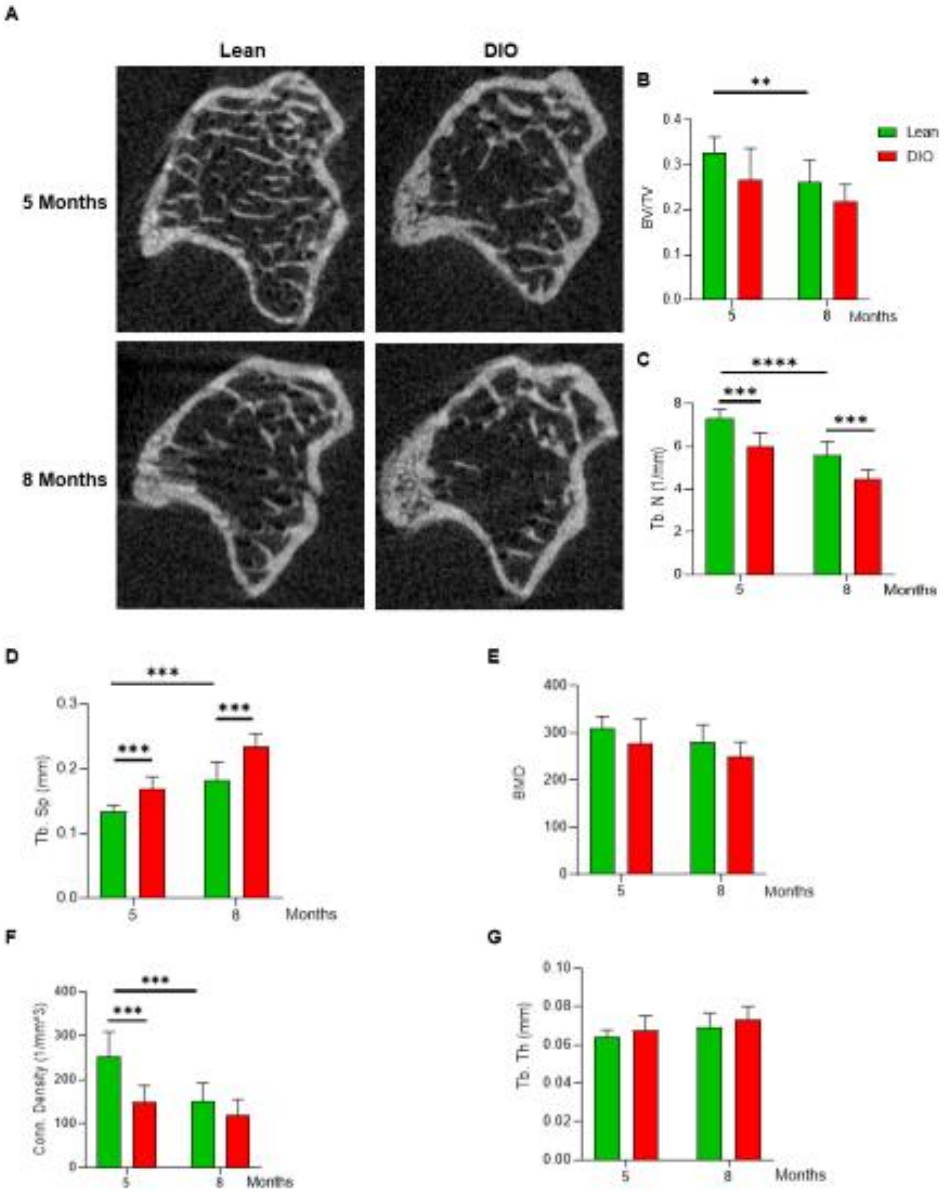

Figure 2.4: µCT analysis of the trabecular tibia. (A) µCT images of trabecular tibia. (B-G) Analysis from the µCT parameters of the trabecular tibia. Results are expressed as mean with +/- SEM, $p < 0.05$ (*), $p < 0.01$ (**), $p < 0.001$ (***), $p < 0.0001$ (****), n=8 or 9.

Another differing result was that there were no significant differences in the BMD between all samples (Figure 2.4: E). The measurement for the Conn.D had statistical significance between the diets of the 5-month-old mice. In addition, there was significance found in a decrease of

Conn.D for lean mice from ages 5 months to 8 months (Figure 2.4: F). Unlike the trabecular femur, there was no significance in Conn.D between DIO and lean mice at 8 months of age.

Regarding the cortical bone, there were no significant differences regarding the Cortical Area (Ct.Area), Bone Mineral Density (BMD), Cortical Thickness (Ct. Th), and the Bone Area to Total Area ratio (BA/TA) (Figure 2.5: B-E).

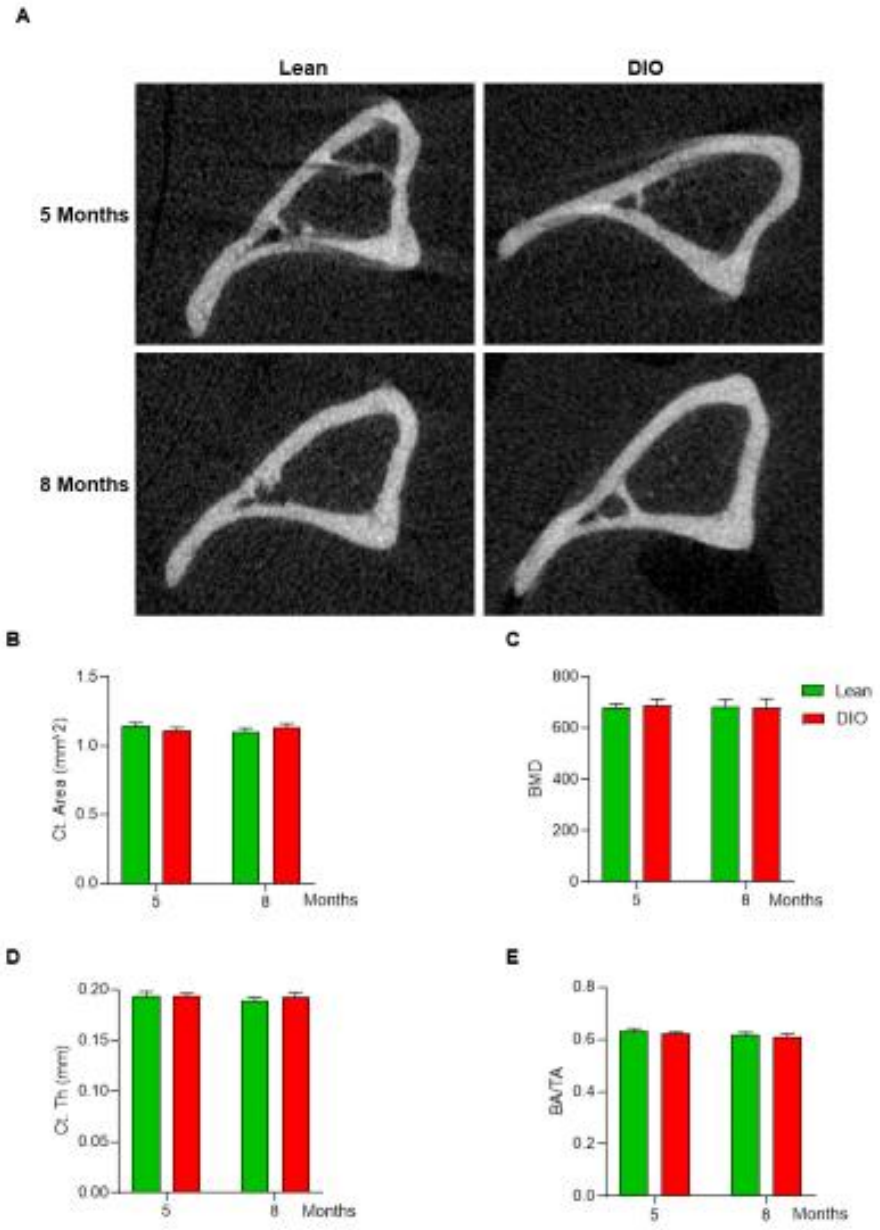

Figure 2.5: µCT analysis of the cortical tibia. (A) representative µCT image of cortical tibia. (B-E) analysis from µCT parameters for cortical tibia. Results are expressed as mean with +/- SEM, n=8 or 9.

Conclusion and Discussion

The secondary structure of the trabecular bone in the tibia and femur were found by μCT imaging to be impacted by obesity. On the other hand, there was no change to the cortical bone secondary structure from obesity.

Obesity has been associated with altering the structure of the bone. The obese mice were found to have a decrease in both BV/TV and Tb.N. when compared to the lean diet (Figure 2.3: B,C and Figure 2.4: B,C). The increased inflammation and a subsequent elevation of inflammatory cytokines in DIO mice could have led to the upregulation of osteoclasts.(2, 4, 5) Increased activity of osteoclasts can correspond to a decrease of trabecular bone, resulting in a difference of BV/TV as well as Tb.N between the lean and DIO groups. The increase in the breakdown of trabecular bone would lead to an increase in the space between trabecular fragments as there would be less trabeculae in the marrow space.

Though the changes to bone secondary structure from obesity alone are unclear in humans, DIO mice in our study followed previously observed trends.(6, 7, 19-22) One of the main areas of concern for humans is the association of obesity with other metabolic conditions and how the BMD is affected. From obesity and associated hyperglycemia, both the femur and tibia trabecular bone had a loss of BMD in the DIO mice (Figure 2.3: E and Figure 2.4: E). The bone loss can be attributed to the increase in total fat percentage (Figure 2.1: A) in the DIO group. One mechanism suggested to be responsible for the decrease in the BMD is due to adipocytes replacing bone. Adipocytes and osteoblasts originate from the same MSCs. During a state of disease the fate of the MSC can be changed.(5, 6, 12, 35) Obesity, especially with hyperglycemia, will increase sclerostin production to increase adipocyte production. The state of hyperglycemia is also responsible for increasing reactive oxygen species to activate the PPAR-γ

pathway for adipogenesis.(5, 11, 36) Bone turnover from the development of adipocytes in the presence of obesity can result in decreased BMD and bone fragility. The differences in the trabecular bone connectivity density can have a relation to the diminished bone integrity from the obesity (Figure 2.3: F and Figure 2.4: F). When the connections between trabeculae are weaker, as a result from bone loss, the bone structure will be compromised.

The cortical bone of the tibia in both DIO and lean mice did not display any significant changes in Ct.Area, Ct.Th, cortical BMD, or cortical BA/TA (Figure 2.5: B-E). Bone alterations can be observed in the trabecular bone of the DIO mice could result from a higher instance of bone metabolism. Trabecular bone is known to be more active as it has a higher level of porosity relative to cortical bone, which increases the surface area for metabolite interactions.(37) As cortical bone is less metabolically active, any affect from obesity on bone may not have culminated by 8-months. Since μCT was unable to detect changes to the mineralized cortical bone, we decided to investigate the organic phase of the bone. This allowed us to assess any influence of obesity the collagen microstructure that could correspond to bone mineralization.

Collagen fibers within the cortical bone were influenced by obesity

One method that allowed the quantitative analysis of the organization of fibrillar collagen was through the use of SHG microscopy.(26-28, 38) By combining two photons of incident light, a single photon with twice the energy and half the wavelength was generated, which made SHG a non-linear optical process.(26-28, 38) For SHG to be effective, only certain types of proteins can be detected. These proteins, like fibrillar collagen, lack a symmetrical center.(26-28, 38) One advantage of SHG was the use of a label-free technique to detect changes in the organization of the fibers when under varying conditions.(26-28, 38) Structural information about collagen features was obtainable through SHG. It allowed the determination of collagen volume fraction,

collagen-fiber orientation (orientation index), and the fiber diameter.(28, 38) When the emitted signal aligned with the excitation signal's direction, this was classified as the Forward SHG (FSHG). Mature collagen fibers emitted 80% to 90% of its signal in the forward direction when used as the medium.(26, 27, 38) On the other hand, the Backwards SHG (BSHG) corresponded to an emitted signal in the backwards direction. This generally represented immature collagen fibrils as their emitted signal aligned with the BSHG.(27, 38) SHG allowed for the determination of the collagen volume fraction and OI.

Multiphoton microscopy was designed to utilize ultra-short IR laser pulses for excitation. The IR laser served as the excitation source to produce multiphoton excitation fluorescence signals from fluorescent complexes, whether endogenous or exogenous.(38, 39) Fluorescence signals from these complexes lead to specific SHG signals.(38, 39)

Collagen volume fraction was analyzed from 3D SHG data sets as described previously.(38, 40) The noise-removal filter (kernel size of 3X3), described above, was applied to assist in analysis of collagen volume fraction. Each region of interest (ROI) was normalized for the fraction by taking all the voxels above the background threshold over the total ROI voxels using Volocity software.

The collagen volume fraction was generated based on the number of voxels above the standard deviation. To determine the percentage of mature collagen fibers, the value for FSHG was divided by the total volume value and then converted to a percentage. The ratio of immature to mature collagen fibers, the values of BSHG were divided by the value of FSHG (BSHG/FSHG). The resulting values were converted to percentages to be standardized for the evaluation of the cortical tibia. Interestingly, analysis of cortical bone indicated that there was a

trend of less precent collagen volume in DIO mice compared to lean mice at 8-months of age (Figure 2.6: A).

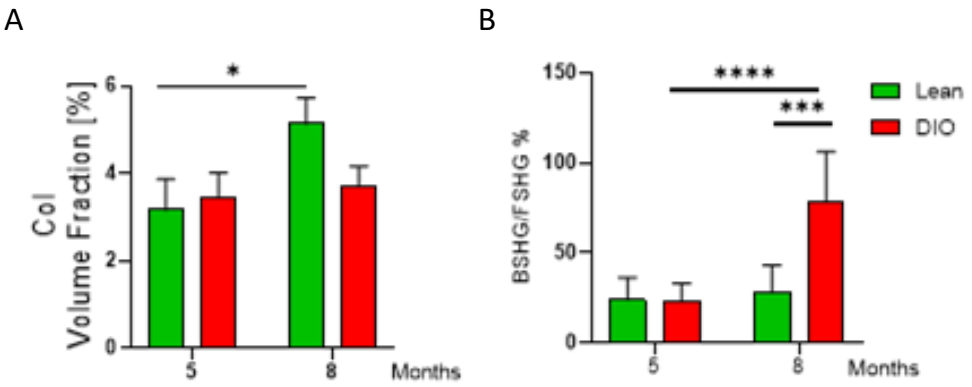

Figure 2.6: SHG results for the collagen volume fraction of the tibia. (A) Cortical tibia. (B) Percentage of backwards to forwards SHG signal ratio for the trabecular tibia. $P < 0.05$ (*), $p < 0.001$ (***), $p < 0.0001$ (****), n=3

Assessment of BSHG/FSHG indicated that there were significantly more immature collagen fibers in the 8-month-old DIO mice. Between the other groups, there was little difference between the type of fibers detected (Figure 2.6: B). These findings complemented the µCT results in the cortical bone. From the µCT analysis, there were no differences observed between the DIO and lean mice in the cortical bone secondary structure (Figure 2.5). Finding elevated immature fibers within the cortical bone from SHG indicated that alterations in the cortical bone may not be observable by µCT in these age groups of mice.

The OI for collagen fibers were calculated using MATLAB (The Math Works) software based on the 2D FSHG and BSHG images as previously described.(28, 38) A MATLAB code was designed to allow the determination of collagen-fiber orientation and anisotropy. The code utilized Fast Fourier Transform (FFT) to covert the collagen fiber spatial patterns in each image into directionally dependent frequency components.(28, 38) The Fourier Transform power spectrum was created and orientation index was determined as described.(28, 38) Orientation index will be computed for the same samples as the collagen volume fraction.

The orientation index represents the percentage of fibers aligned in a specific direction. The MATLAB software and Fourier Transform allowed utilization of the 2D image and the degree of collagen fiber orientation.(28) The closer the values are to 100%, indicates that the values obtained from all the fibers in an image are aligned in a certain direction. When the values are closer to 0%, this corresponds with the all the fibers from an image being randomly aligned.(28) The OI for the cortical tibia of the 5-month-old mice showed significantly more organized collagen fibers than the 5-month-DIO mice (Figure 2.7).

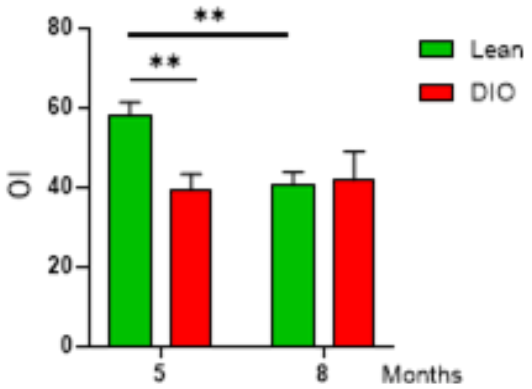

Figure 2.7: SHG results for the collagen orientation index as a percentage of cortical tibia. Results are expresses as mean with +/- SEM, $p < 0.01$ (**), n=3.

For lean mice, there was a significant decrease in fiber organization from 5-months to 8-months. In DIO mice, there was no significant difference with fiber organization from 5-months to 8-months (Figure 2.7). The OI results indicate that obesity can impact the organization of the collagen fibers in the cortical bone of the tibia.

Conclusion and discussion

The impact of obesity on cortical bone was only at the collagen level as determined by SHG microscopy. Collagen fibers of the cortical bone were more immature and disorganized in DIO samples.

The influence of obesity on the trabecular bone of the tibia was determined to have significant impact on the BV/TV, Tb.N, and Tb.Sp (Figure 2.4: B-D). Tibial cortical bone,

however, through μCT analysis determined that there was no impact of obesity (Figure 2.5: B-E). Since SHG has the ability to allow for the quantitative analysis of collagen fiber microstructure, we evaluated the collagen fibers of the cortical tibia. The signals obtained through SHG microscopy of collagen relied on the spatial distribution and organization of the collagen molecules.(40) Tissues can depend on the foundational organization of the collagen as collagen type I fibers make up roughly 90% of the organic component to the bone.(41) Any pathological influence may require the remodeling of the pre-existing collagen matrix.(28) When comparing the BSHG/FSHG, 8-month-old DIO group had significantly more immature fibers, while the other groups had generally the same ratio. One mechanism responsible for the lack of mature fibers could result from the development of advanced glycation end products (AGEs).(42) The development of AGEs within collagen result from a post-translational modification to the collagen as a result from covalent bonds between reducing sugars and free amino groups.(24, 25) This mechanism generally leads to changes in the cross-link density of the collagen throughout aging.(25, 42)

According to the results in Figure 2.7, the cortical tibia had more fibers oriented in a similar direction for the 5-month-old lean samples. The significant decrease in organization the lean mice from 5-months to 8-months could be a result from natural development of AGEs. By weakening the cross-link interactions, more fibers could have varying orientations and compromise the bone structure.(24, 25) The level of disorganization in collagen fibers from five to eight months in lean mice was reached by five months in DIO mice (Figure 2.7). This indicated that the collagen fibers of the cortical tibia in DIO mice had accelerated changes to the organization.

Summary

Microcomputed tomography provided the ability to evaluate the bone structure in mice. The trabecular bone of both the distal femur and proximal tibia was found to have been altered in obese mice. Between the two locations of trabecular bone, there were similar changes to the trabecular features although more significant differences were found in the femur than tibia. Obesity appeared to have a negative impact on the bone structure from μCT evaluation. As the cortical bone had little change detectable by μCT imaging, we pursued evaluating cortical bone collagen organization using SHG. We found that 8-month-old DIO samples had more immature fibers and 5-month-old DIO samples had accelerated disorganization of the collagen fiber. These results indicate that changes in the collagen microstructure from obesity may not have a detectable impact on the structure of cortical bone by 8-months. SHG microscopy was a valuable tool to evaluate the bone structure at the collagen level. The cortical tibia was found to have a negative influence from obesity on the collagen fiber microstructure. As SHG indicated that the collagen fibers were affected by obesity, this may not directly associate with detectable changes in the cortical bone. The μCT assessed the mineralized cortical bone, while the SHG evaluated the organic component of the cortical bone. Even though type I collagen has a role in bone mineralization, the effect of obesity in cortical bone was not yet detectable by μCT as it was by SHG.

Chapter 3: Impact of Obesity at the Cellular Level

Changes in the bone structure were found to be associated with a state of obesity in mice. Alterations in the trabecular bone were quantified by μCT. Any changes to the cortical bone were only detectable at the collagen level. Since the bone structure was affected by obesity, investigations into the mechanisms were required.

Evaluation of TNF-α throughout the bone marrow in obese mice

To evaluate the obesity mechanism leading to alterations of the bone, immunofluorescent (IF) staining was performed. Tumor necrosis factor alpha (TNF-α) is pro-inflammatory cytokine that has been found to be associated with chronic inflammation.(2, 4-7) The connection is through the RANK/RANKL/OPG pathway as inflammatory cytokines can influence osteoclast differentiation from MSCs as described above.(4) Elevated TNF-α levels from chronic inflammation also has an effect on GLUT4. This insulin-regulated glucose transporter is known to be associated with adipocytes and skeletal muscle.(43) The constant presence of TNF-α has been found to lead to insulin resistance by inhibiting the action of insulin on GLUT4.(43) As the DIO mice are insulin resistant, they were speculated to have elevated levels of TNF-α. By determining the amount of TNF-α in the bone samples, any association between bone health and TNF-α could be further evaluated.

The IF-staining routine followed a standardized procedure. Bone histological samples were taken from 5-month-old lean and DIO mice, as well as 8-month-old mice with the same respective diets. For staining, 5μm thick sagittal sections were taken from the decalcified, paraffin block. Sections were taken to include the distal femur, knee-joint, and the proximal tibia. For the four test groups, there was one section used for each of the five different samples. Paraffin was solubilized in three washes of Xylene for five minutes. The solubilized paraffin was removed using gradient washes of EtOH: two washes at 100% for five minutes, two washes at

95% for five minutes, and one wash at 70% for 2 minutes. Following the removal of the paraffin, the sections were rehydrated using DH_20 for two washes at one minute. After rehydration, the sections were placed in 1X TBS buffer to prevent drying until the antigen retrieval step.

Antigen retrieval procedures were optimized according to the primary antibody being used. To permeabilize the cellular membrane, the sections were placed in 0.03% Triton®-X for 30 minutes. 10% Normal Goat Serum (NGS) in 1X TBS was used for blocking of the samples and incubated at RT for two hours. Application of primary antibody corresponded to the recommended dilution with incubation occurring at 4ºC overnight.

Application of secondary antibody began with three washes of 1X TBS for five minutes each. Biotin-Streptavidin conjugated with Alexa fluor 647 was used to allow detection via immunofluorescence. A biotinylated goat anti-rabbit secondary antibody was applied to allow for fluorescence. Each sample was incubated for one hour at RT with the biotin solution. Following incubation were three washes of 1X TBS for five minutes each. The secondary antibody was applied to each slide for incubation at RT in the dark. The slides were then washed in 1X TBS for five minutes, three times. The slides were submerged in 0.03% Triton®-X for five minutes and then another two, five-minute washes in 1X TBS.

Mounting was done with ProLong™ Gold antifade reagent with DAPI (Invitrogen) by applying one drop onto the sample followed by a coverslip. After allowing the samples to air-dry overnight, the coverslips were sealed using clear nail polish. The samples were stored in the dark at 4ºC. Zeiss Axio Observer 7 upright wide-field microscope (Carl Zeiss Microscopy GmbH) was used for imaging of the stained sections. Zeiss Blue edition image analysis software allowed for the analysis of area positive signal.

Quantitative analysis was performed through the analysis feature of the Zeiss program. Manual contouring was done to outline the areas of interest. The threshold corresponding to the signal was adjusted and standardized between all samples to allow for comparison. The area of signal was determined from the program analysis feature. The average percent area was calculated within all groups. For statistical analysis, a student's t-test was used to determine significance.

The detailed IF-staining procedure for TNF-α can be found in Appendix A. Analysis of the TNF-α was done through the Zeiss Analysis program. The TNF-α area was evaluated by measuring the positive signal throughout the regions of interest. The TNF-α signal was represented by the green signal, while all cellular nuclei were colored blue (Figure 3.1: A).

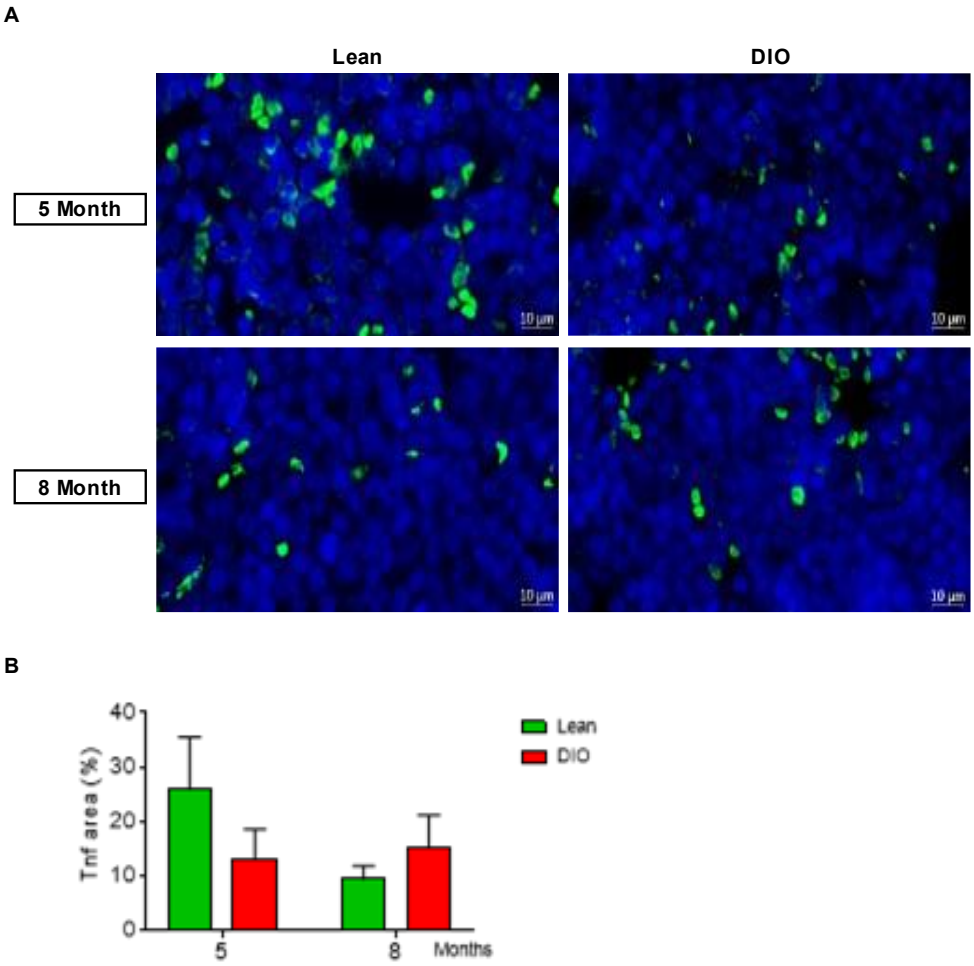

Figure 3.1: IF-staining for the detection of TNF-α throughout bone marrow of the distal femur. (A) IF images of positive TNF-α areas in green, cellular nuclei in blue. (B) Quantitative analysis of positive TNF-α signal throughout the bone marrow, n=4 or 5.

Quantitative analysis indicated that the presence of TNF-α was the highest in 5-month-old lean mice, though insignificant (Figure 3.1: B). Comparing 5-month-old to 8-month-old lean mice, the percentage of TNF-α area was indicated to decrease. On the other hand, the DIO mice appeared to have an increase in the inflammatory cytokine from 5-months to 8-months (Figure 3.1: B).

TNF-α is known to be a product of macrophage response to injury, inflammation, or infection. An influence on bone from TNF-α expression could result in the overproduction of osteoclasts by inhibition of the RANK/RANKL/OPG pathway.(4) According to the IF-staining results, there was a trend for a decrease of TNF-α in lean mice bone marrow from 5-months to 8-

months (Figure 3.1: B). The trend of a decrease of TNF-α from 5-months to 8-months indicate that levels could naturally decrease. On the other hand, there was no significant change in TNF-α from 5-months to 8-months for the DIO mice. Any prolonged state of obesity has been found to lead to increased inflammation and inflammatory cytokines.(2, 4-7) The results of the TNF-α IF-stain indicate that this inflammatory cytokine was not found to be correlated with the changes in the bone at these two age groups. Since this one pro-inflammatory cytokine showed insignificance throughout the bone, proteomics was used to explore the presence of other proteins within bone samples.

Proteomics determined differences in proteins between groups

Entire bone samples were pulverized and sent to the Mass Spectrometry and Proteomics Core Facility at Penn State College of Medicine for proteomic analysis. Proteomics allow for the determination of what proteins were differentially expressed between the lean and DIO groups.(44) Four samples from both DIO and lean diet groups were analyzed. Analysis of peptide and proteins levels were performed through the use of Scaffold Q+ (version Scaffold_4.11.0, Proteome Software Inc., Portland, OR) Label Based Quantitation (iTRAQ). Once peptides and proteins were identified, their identities were verified by having the Scaffold Local FDR algorithm applied. Accepted peptide identities had a probability value greater than 95.0%. For protein identifications to be accepted, at least 2 peptides were needed to be identified and a probability of 99.0% established by the Protein Prophet algorithm.(45) When proteins contained similar peptides, mass spectrometry/mass spectrometry (MS/MS) analysis was used for differentiation. If the proteins containing similar peptides could not be differentiated by MS/MS, then these proteins were grouped to satisfy the principles of parsimony. Proteins were placed into clusters when there was significant evidence of peptides being shared. Channels were

corrected by the matrix: [0.000,0.000,0.929,0.0689,0.00240]; [0.000,0.00940,0.930,0.0590,0.00160]; [0.000,0.0188,0.931,0.0490,0.001000]; [0.000,0.0282,0.932,0.0390,0.000700]; [0.000600,0.0377,0.933,0.0288,0.000]; [0.000900,0.0471,0.933,0.0191,0.000]; [0.00140,0.0566,0.933,0.00870,0.000]; [0.00270,0.0744,0.921,0.00180,0.000] in all samples according to the algorithm described in i-Tracker to assist with identification.(46)

Normalization was performed iteratively (across samples and spectra) on intensities using ANOVA, as described.(47) Averages were calculated from the medians. Spectra data were log-transformed, pruned of those matched to multiple proteins, and weighted by an adaptive intensity weighting algorithm. Of 29339 spectra in the experiment at the given thresholds, 2497 (9%) were included in quantitation. Differentially expressed proteins were determined by applying Mann-Whitney Test with unadjusted significance level $p < 0.05$ corrected by Benjamini-Hochberg.

For the proteomic analysis, the upregulated proteins were calculated by a positive Log2 fold change value. This value was determined by being compared to the value for the same protein in the lean sample. The five most upregulated proteins can be found in Table 3.1.

Top 5 Identified Proteins (upregulated and downregulated)	Log2 Fold Change (DIO /lean)
Upregulated	
lumican precursor	7.82
protein S100-A10	5.62
catalase	5.59
predicted gene 4737	4.64
ubiquitin carboxyl-terminal hydrolase isozyme L3	4.6
Downregulated	
BTB/POZ domain-containing protein KCTD12	-6.4
eukaryotic translation initiation factor 3 subunit M	-6.3
protein-glutamine gamma-glutamyltransferase 2	-6.03
P04258 SWISS-PROT:P04258 (Bos taurus) Similar to Collagen alpha 1(III) chain	-6
isocitrate dehydrogenase [NADP] cytoplasmic	-5.89

Table 3.1: Quantitative proteomic analysis results for upregulated and down regulated proteins between DIO and lean mice. Shown are the five most upregulated and five most downregulated.

A Lumican precusor was found to be the most upregulated protein in the DIO samples by having a log2 fold change value of 7.82. On the other hand, the five most downregulated proteins were

determined as well. It was found that BTB/POZ domain-containing protein KCTD12 was the most downregulated protein in DIO mice with a value of -6.4 (Table 3.1).

Our interest in proteomics resided in any protein that was detected to have a substantial upregulation in the DIO samples compared to the lean group. As the lumican precusor was found to have more upregulated in DIO mice, this directed the experimental procedure. The goal would be to determine why this protein was elevated and the role it has on bone homeostasis.

Lumican was detectable in the distal femur by IF-staining

Lumican expression can be throughout the bone matrix. The lumican expression has been reported in mature and developing osteoblasts, with the former having more expression.(48) The proteoglycan has been associated with metastasis as well as tumorigenesis in different types of cancer.(29) The ability of lung cancer cells to metastasize to the bone has been found to be possible by lumican.(49) As lumican has been linked to the bone previously, we decided to further explore the bone for a potential connection to obesity. IF-staining was conducted for the detection of lumican following the detailed protocol in Appendix B. For each group, five samples were taken and stained to assess the presence of lumican in the distal femur.

Analysis of the Lumican signaling was completed using the analysis feature of Zeiss Blue Edition 2.6 software. The percent area of positive signal was determined from the entire contoured area. The average for each sample group was calculated with student's t-test being used for statistical analysis. Lumican was analyzed in the bone marrow, trabecular femur, and cortical tibia. The percent area of Lumican within the bone marrow was significantly higher in the 5-month-old DIO group than the respective lean group (Figure 3.2: B).

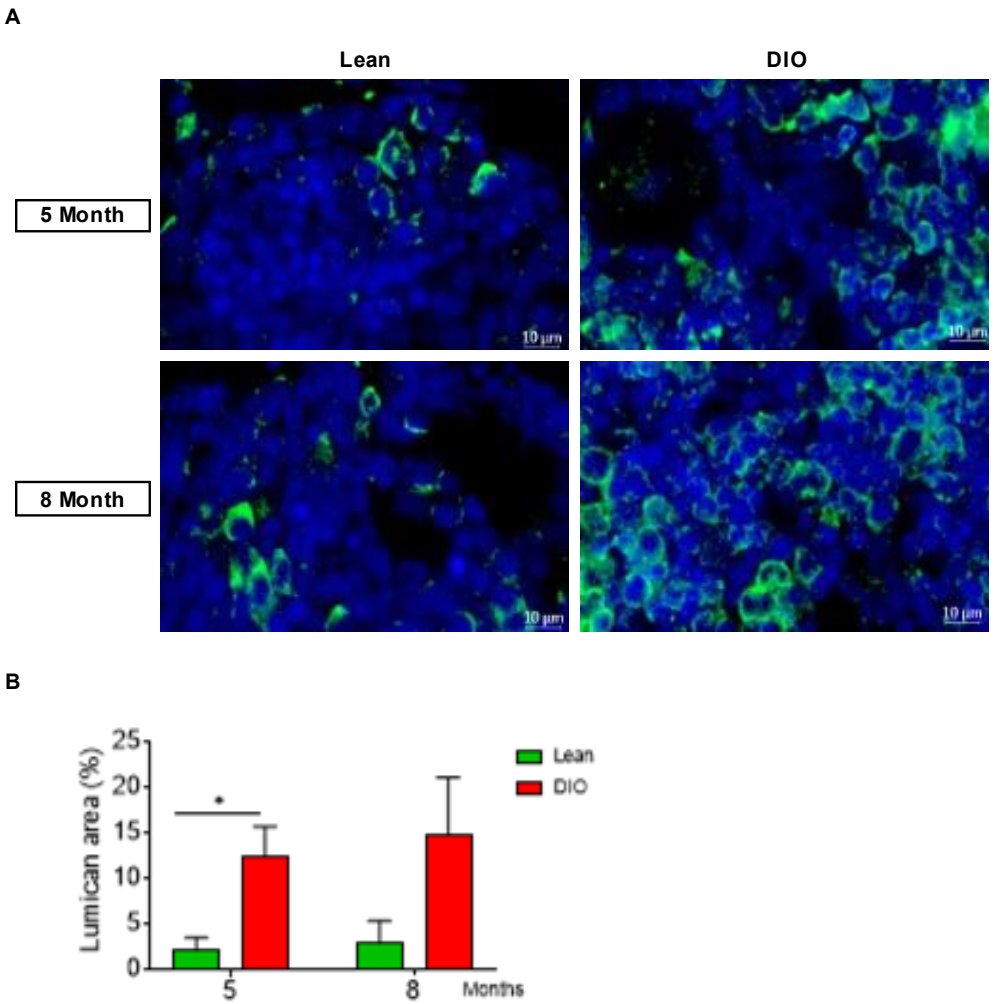

Figure 3.2: Lumican expression in the distal femur bone marrow. (A) IF images taken at 40x magnification of bone marrow for each group with lumican areas represented by green and cellular nuclei as blue. (B) Quantitative analysis of the lumican expression in the bone marrow. Results are expresses as mean with +/- SEM, $p < 0.01$ (*), n=3.

Though insignificant, the data showed that the 8-month-old DIO group had a larger percent area of Lumican than the respective lean group. Within the dietary groups, there appears to only be a slight increase as the mice age even though it was insignificant (Figure 3.2: B).

While looking at the bone lining cells and osteoblasts specifically, there was a significant increase of percent area Lumican for the 8-month-old DIO group compared to the 8-month-old lean group (Figure 3.3: B).

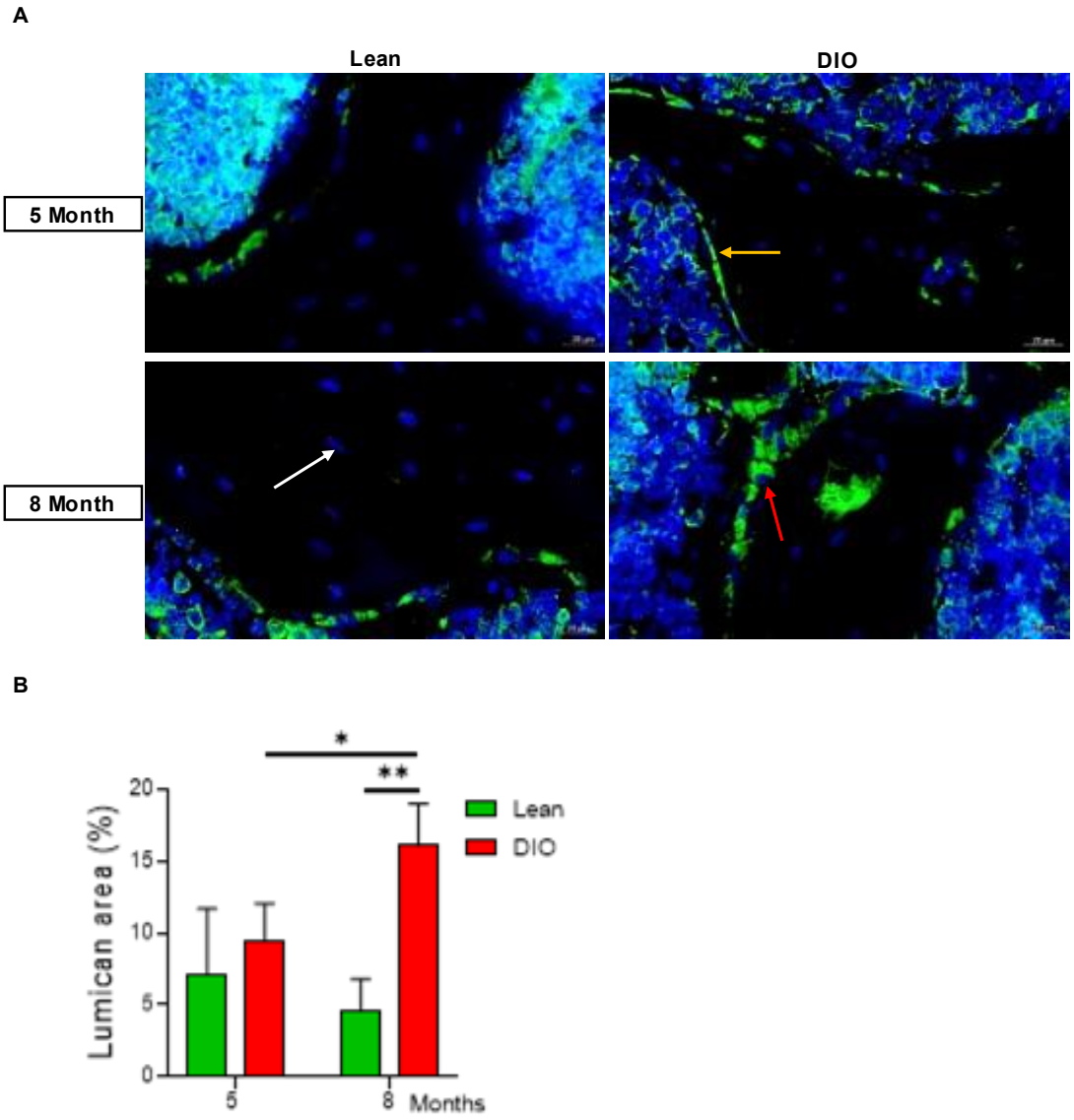

Figure 3.3: Lumican expression of the cells associated with trabecular bone within the distal femur. (A) IF images taken at 40x magnification with lumican areas represented by green and cellular nuclei as blue. (B) Quantitative analysis of the cells that are associated with the trabecular bone. Results are expresses as mean with +/- SEM, $p < 0.05$ (*), $p < 0.01$ (**), n=3.

Within the DIO group, there an increase of Lumican percent area when comparing the 8-month-old to the 5-month-old (Figure 3.3: B). During evaluation of the cortical bone, there was no lumican expression detected.

qPCR verified lumican expression in trabecular bone and bone marrow

To verify the IF-staining results of lumican throughout the trabecular tissue, qPCR analysis was performed to detect expression levels. Tibia and femur were harvested as previously

described. The distal femur and proximal tibia were briefly dipped into a small volume of RNALater to preserve the RNA within the bone. The samples were then flash-frozen in liquid nitrogen to be stored. The bone marrow was flushed using a 27g, ½-inch needle with 1X DPBS. Samples were centrifuged at 1,500 rpm for 5 minutes to spin down bone marrow cells. The supernatant was removed and then the cells were flash-frozen if not to be used immediately. Similarly, cortical bone was placed in a small volume of RNALater, then flash-frozen to be stored in liquid nitrogen. The RNA extraction was done using TRIzol™ (ThermoFisher Scientific) following manufacturers protocol. DNA removal from samples was performed using a TURBO DNA-*free*™ Kit (ThermoFisher Scientific) following the followed the Routine DNase Treatment section within the manufacturers protocol. Concentration and purity were verified using the NanoDrop™ and can be found in Appendix E. Reverse transcription was done using iScript™ cDNA synthesis kit and 500-750ng of RNA. The thermocycler program for RT was as follows: priming was done at 25ºC for five minutes. Reverse transcription was done at 46ºC for 20 minutes. Inactivation of the reverse transcriptase was done at 95ºC for one minute. Infinite holding was at 4ºC until storage at -20ºC.

TaqMan gene expression assay was used for qPCR for the quick amplification of the targeted gene. 2X TaqMan DNA polymerase was used in conjunction with 20X TaqMan primers probes for the gene of interest. The endogenous control for reference was β-Actin, while the Lumican gene was the target. qPCR was done using StepOnePlus with a fast reaction time of roughly 40 minutes. For quantification, a comparative $\Delta\Delta C_T$ was used to determine the number of cycles required to reach the threshold of gene expression. 96-well plates were used for qPCR. Amplification occurred over 40 cycles: Activation at 95°C for 20s, denaturation at 95°C for 1s,

and annealing/extension at 60°C for 20s. Quantitative analysis was calculated within the StepOnePlus program using the ΔΔCt mode to give relative expression of desired gene.

Lumican expression for the trabecular bone was evaluated. Within the 5-month-old group, it was indicated that there was more lumican expression in the DIO mice (Figure 3.4)

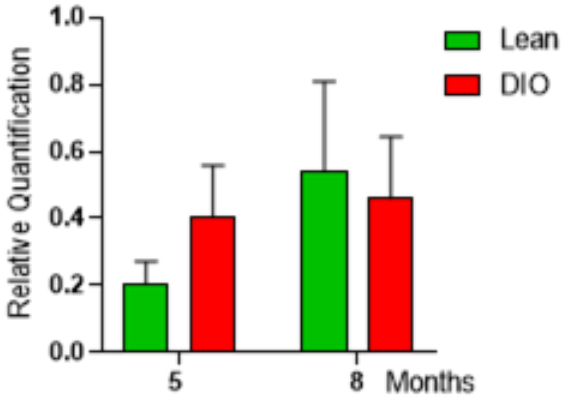

Figure 3.4: Relative quantification of lumican expression in the trabecular bone of the distal femur. Results are expressed as mean with +/- SEM, n=4 or 5.

There was a trend of increased lumican expression from 5-months to 8-months (Figure 3.4). As the age increased from 5 to 8 months, there was no significant increase of lumican expression in DIO mice. All of the results for this experiment were insignificant yet, the difference between within the 5-month-old group was of further interest. Lumican has been reported to be associated with bone, however little is known about the protein in the bone marrow.

Following the results of the IF-staining and qPCR of trabecular tissue, the next step in the experimental procedure was to assess the lumican levels in bone marrow. One lean mouse and one DIO mouse were sacrificed and had the bone marrow flushed from the femur and tibia to ensure enough cells for RNA extraction. Following bone marrow purification, RNA extraction was executed following the protocol described above. To prepare for qPCR, cDNA was

developed following a similar method as described previously. qPCR results indicated substantially elevated lumican expression in the DIO sample as compared to lean (Figure 3.5).

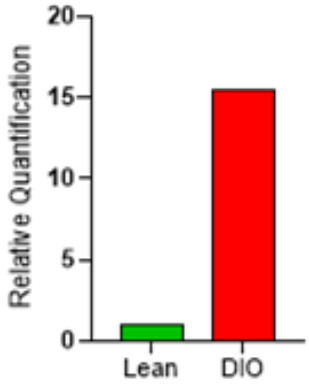

Figure 3.5: Relative quantification of lumican expression of the bone marrow, n=1.

This finding would need verification from other samples within the respective diet and age groups. The results suggested that elevated lumican is correlated with obesity.

Conclusion and discussion

Within the bone marrow, the percentage of lumican area was elevated in obese mice when compared to the lean mice. The expression of lumican in the bone marrow of obese mice was confirmed by qPCR analysis. Bone marrow from mice that were 5 months old showed the largest difference of lumican by IF-staining and qPCR.

From the IF-staining, Lumican was detectable throughout the trabecular bone and bone marrow of the distal femur. Obese mice were found to have more percent area of lumican. In Figure 3.2: B, the DIO mice in both age groups had a higher percentage of lumican within the bone marrow. When cellular features of the trabecular bone were evaluated, there was on average significantly higher percent lumican area in 8-month-old DIO mice when compared to the other groups (Figure 3.3: B). The cells associated with the trabecular bone are the osteocytes, osteoblasts, osteoclasts, and bone lining cells. A group of non-collagenous proteins, proteoglycans, are produced by the cells of the bone.(50) When proteoglycans interact with collagen, they can regulate collagen fiber diameter and potentially serve a role in bone

mineralization.(50) As lumican is a proteoglycan, it may be a factor in this process. Due to being differentiated within mineralized bone, osteocytes are found to not express lumican.(50) Since lumican has been referenced to be connected to cell fates, we decided to evaluate if lumican was associated with apoptosis.

Summary

TNF-alpha was found to not be associated with bone alteration for 5-month-old and 8-month-old DIO or lean mice. Proteomic analysis was performed on ground-bone samples from both diet groups. The results indicated that of the many varying proteins found, an extracellular matrix proteoglycan was found to be the most upregulated in DIO mice compared lean mice.

Preliminary data from qPCR provided the verification that lumican is elevated in the bone marrow of obese samples. As lumican was detected in the bone marrow, being able to isolate which cells express lumican could allude to the role it has throughout the bone.

Chapter 4: Identification of Bone Marrow Cells That Express Lumican

Lumican expression was detected in the bone marrow of the distal femur. Regions that expressed lumican were established by IF-staining. Verification of lumican throughout regions of interest was confirmed by qPCR. To determine the role of lumican further IF-staining and experimentation was utilized.

TUNEL assay detected the percentage of apoptotic cells

Lumican has been previously reported to be associated with apoptosis. *In vitro* mouse embryonic fibroblasts (MEFs) throughout the cornea was found to have more cell proliferation and decreased apoptosis in lumican null mice.(51) These mice were also found to have a decrease in Fas receptors and presentation of Fas ligand.(51, 52) Fas receptor is a member of the tumor necrosis factor receptor superfamily that can be localized on various cell surfaces. As a member of the TNF superfamily, this death receptor has a cytoplasmic death domain.(53) When the death receptor is bound, it can recruit Fas-associated protein with death domain (FADD).(53) When Fas ligand binds to its receptor, it will trigger pathways that lead to apoptosis by activation of caspase-8 and capase-10.(53) Another cell line, murine brain microvascular endothelial cells, displayed elevated capsase activity when in the presence of lumican *in vitro* which led to apoptosis.(52)

For the detection of apoptotic cells in the bone marrow, a Terminal deoxynucleotidyl transferase dUTP Nick-End Labeling (TUNEL) Assay was performed following an adapted protocol for the Click-IT® Plus TUNEL Assay kit (ThermoFisher Scientific). Apoptosis is programmed cellular death that can be activated by chemical stimuli as well as other factors.(54) Cell death traditionally results in fragmented DNA. Once the fragmented DNA is exposed, the 3’-OH end of the DNA interacts with dUTP to allow for visualization.(54)

Samples were deparaffinized as described above. Proteinase K was used for the permeabilization of the samples between two tissue fixation steps with 4% Paraformaldehyde (PFA). TdT reaction facilitated the labelling of fragmented DNA. For the visibility of apoptotic cells, the Click-IT® Plus reaction allowed binding of an immunofluorescent Alexa Fluor. A detailed protocol can be found in Appendix C. Images and analysis were obtained via Zeiss Microscope as well. The analysis required the use of the Zeiss program to count the DAPI positive cells. Manual counting of positive cells which co-localized with DAPI positive cells corresponded to the indication of cellular apoptosis. Analysis only consisted of the cells that were completely co-localized as this represented a specific stage of apoptosis.

For the TUNEL Assay, the DIO groups had substantially more apoptotic cells. When comparing the 5-month-old groups, there was significantly more apoptotic cells in the DIO group than the lean group (Figure 4.1: B).

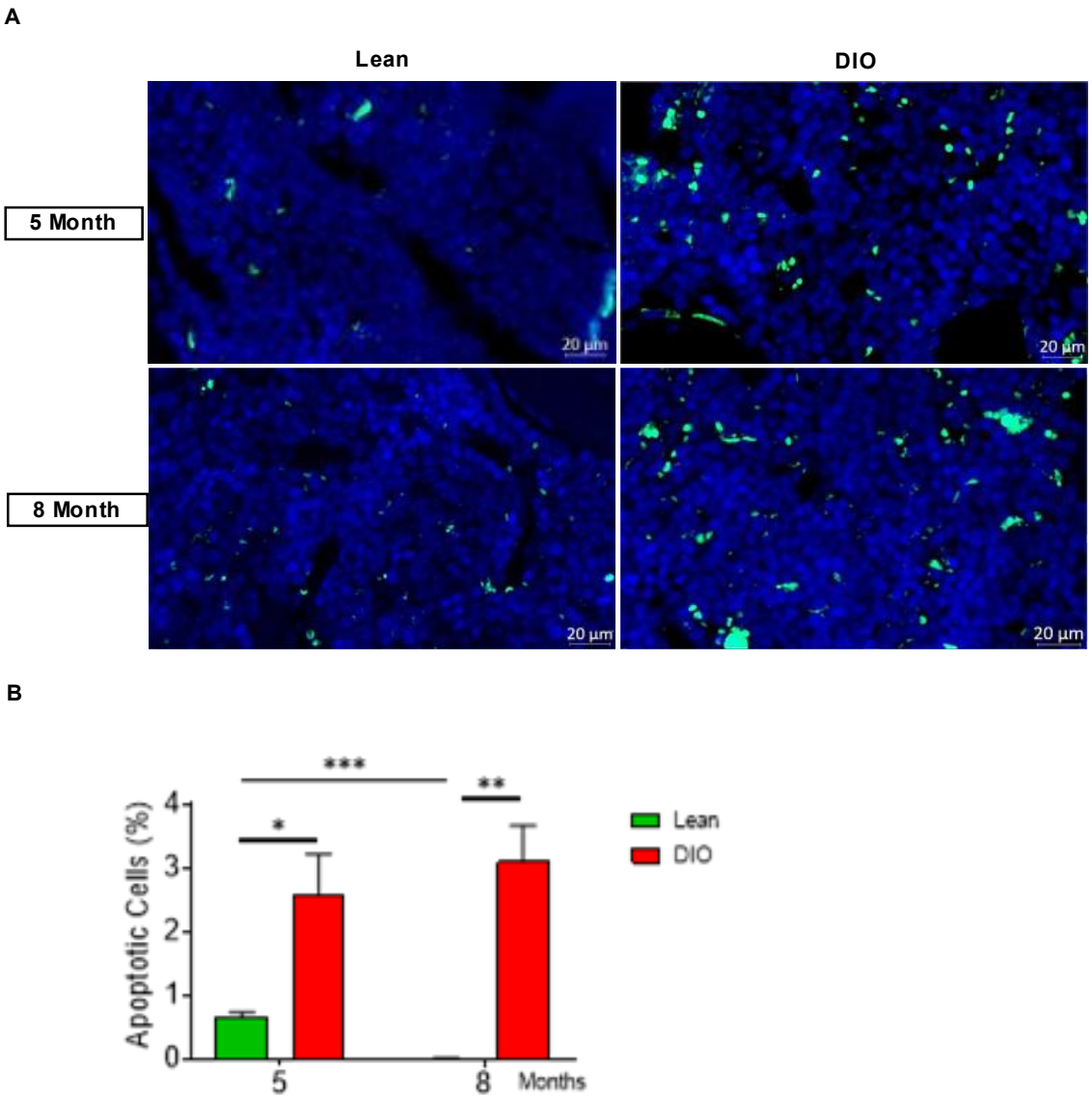

Figure 4.1: TUNEL assay imaging and analysis of the apoptotic cells in the distal femur bone marrow. (A) IF imaging of the distal femur bone marrow with apoptotic cells represented by green and cellular nuclei as blue. (B) Quantitative analysis of the percentage of apoptotic cells within the distal femur bone marrow. Results are expresses as mean with +/- SEM, $p < 0.05$ (*), $p < 0.01$ (**), $p < 0.001$ (***), n=4.

Within the 8-month-old group, there was significantly more apoptotic cells in the DIO group compared to the lean group (Figure 4.1: B). When comparing the age groups within the lean diet group, there were more apoptotic cells at 5-months, than at 8-months (Figure 4.1: B). There was a significant increase of apoptotic cells between the 5-month-old DIO group and the 8-month-old

lean group (Figure 4.1: B). There was also significant increase of positive staining in the 8-month-old DIO group and 5-month-old lean group (Figure 4.1: B).

Regions with elevated lumican in DIO mice had higher instances of apoptosis

Based on the results of from the TUNEL Assay, there was consideration to develop a co-staining technique to evaluate if there was co-localization between lumican and apoptotic cells. The procedures were not feasible as the permeabilization steps were incompatible for both proteins. This led to the decision to stain serial sections to consider if the region of high lumican expression corresponded with excess apoptosis within the same region. The lumican staining procedure was executed as described above and in Appendix B. The subsequent histology section for each sample was used for the TUNEL assay, which was stained as described above and in appendix C.

In Figure 4.2, lumican was represented by the magenta color, cellular nuclei were blue, and the apoptotic cells were green.

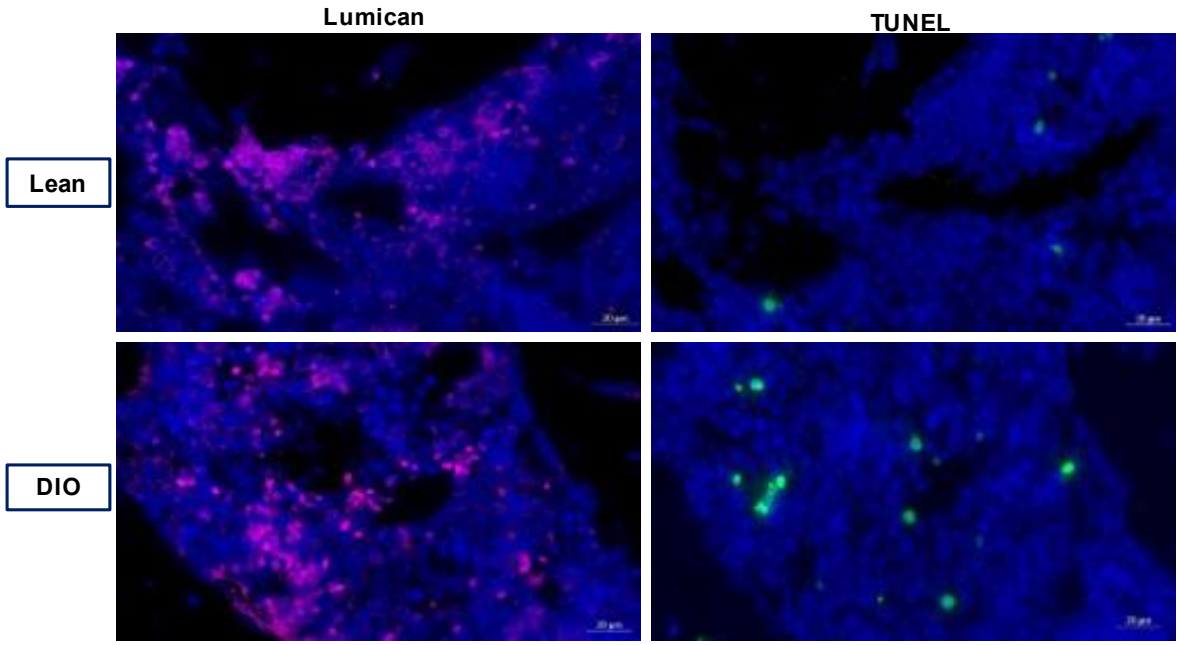

Figure 4.2: IF imaging of sequential sections for the detection of TUNEL expression in ROIs with lumican expression. Samples are from 5-month-old lean and DIO mice. TUNEL (green) and lumican (magenta) imaged at 647nm, n=5.

The DIO samples appeared to have more apoptosis in regions with elevated with lumican expression (Figure 4.2). There was no indication that the same cells that were apoptotic expressed lumican (Figure 4.2).

Conclusion and discussion

Obese samples were found to have an increased percentage of apoptotic bone marrow cells. Elevated lumican expression appeared to be correlated with apoptosis in obese samples.

The function of lumican in these regions may have contributed to the apoptosis. Extracellular matrix proteins have been found to play a role in cellular fates, specifically apoptosis.(29) Elevated lumican has been reported to increase the presence of fas receptors.(52) The fas-mediated apoptosis is triggered by following the activation of caspase. Death receptors (DRs) interact with fas-ligand which lead to the increase in the caspase activity.(53) The activity of caspase results from DRs recruiting death domains (DDs). As these DDs become associated with Fas, FADD, they will recruit caspases to initiate the apoptotic pathway.(53) Regions of bone marrow that had elevated lumican expression were only found to have more apoptotic cells for DIO mice. This finding may indicate that elevated lumican could potentially be associated with cellular apoptosis. Whether lumican was a result of apoptosis, or a trigger was undetermined. It was reported that apoptosis is a common cell fate for adipocytes when in an obese metabolic state. The DIO samples were found to have more apoptotic cells. In a state of obesity, MSCs can have an altered differentiated pathway. They have the ability to become osteoblasts or adipocytes.(2, 4) The bone marrow cells could produce lumican as restorative response towards the development of adipose tissue. To prevent the adipose tissue from further developing in the bone marrow, lumican could induce apoptosis to help preserve the bone marrow niche. To confirm the role of lumican, further exploration of which cells express the

proteoglycan and what results of the expression. Isolation of MSCs in cell culture can help determine lumican's roll in differentiation and apoptotic potential.

Fluorescent-activated cell sorting for bone marrow stromal cells

To evaluate which cell population expresses lumican, FACS analysis was performed on bone marrow cells. On a WT, lean diet mouse around 5-months-old, both lower extremities were harvested. Bone marrow from the cortical femur and tibia were flushed. The cells were resuspended to be filtered the cells were filtered using a 70µm nylon mesh filter. Red Blood Cell lysis buffer was used to remove unwanted RBCs. To prepare the samples for FACS, the cells were incubated with a volume of Brilliant Violet 650™ anti-mouse CD45 Antibody per million cells. The CD45 antibody is a marker for hematopoietic stem cells.(55) The goal was to isolate the CD45 negative cells from the positive to study the bone marrow stromal cells.

After receiving both cell populations, RNA extraction was performed following the procedure as described above. Generation of cDNA from the RNA was executed following the method as previously described. The cDNA from both populations were used for qPCR analysis. We were investigating to see if lumican would be expressed from either of these sub-populations. We hypothesize that CD45(-) cells will express lumican as these cells contribute to the stromal fraction. The gating and qPCR results can be found in Figure 4.3. Lumican was found to be expressed in CD45(-) cells; indicating that bone marrow stromal cells express lumican.

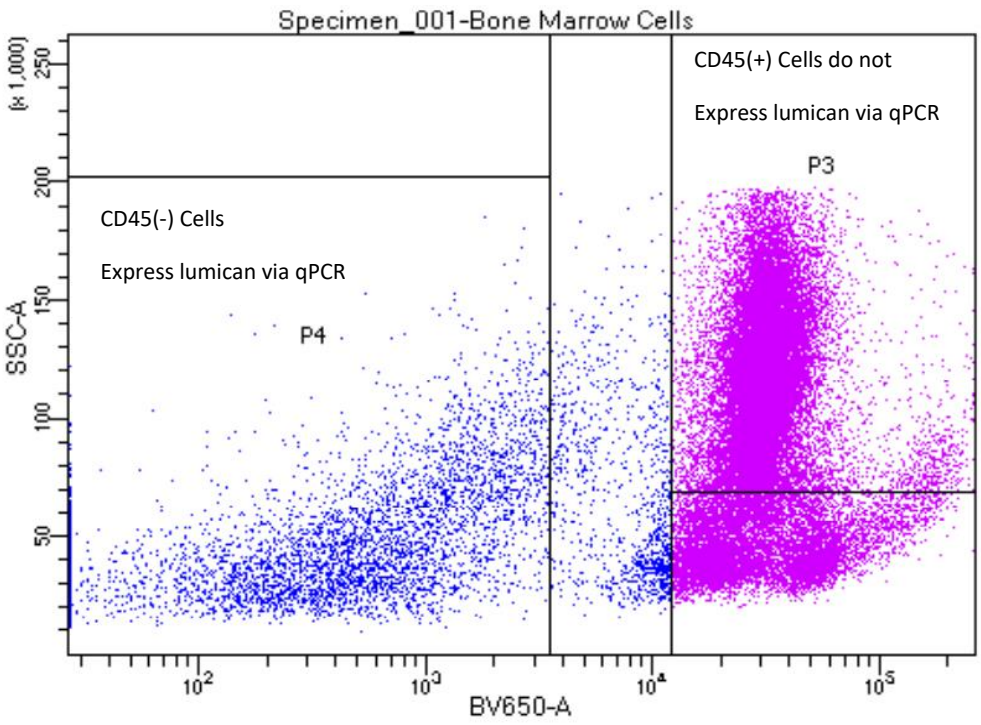

Tube: Bone Marrow Cells

Population	#Events	%Parent	%Total
All Events	58,637	####	100.0
P1	43,219	73.7	73.7
P2	42,052	97.3	71.7
P3	35,421	84.2	60.4
P4	5,608	13.3	9.6

Figure 4.3: Gating for the FACS of Bone Marrow cells. P3 represents the cell population of CD45(+) cells. P4 represents the cell population of CD45(-) cells.

Exploration if MSCs express lumican

For the determination of what cells in the stromal fraction express lumican, we IF-costained for lumican and a MSC marker, Sca-1. The co-localization of lumican with MSCs followed a similar staining protocol as describe above. Tissue sections of the test groups were selected from the same tissue level as previous staining procedures. Deparaffinization of the sections followed the same procedure as described above. To prevent unspecific binding of primary antibody, 10% NGS was used for blocking. The Sca-1 primary antibody utilized a conjugated antibody with an Alexa Fluor® for detection. After overnight incubation, the samples

were washed in 1X TBS. Following the wash, the incubation step with lumican primary antibody on the second day was performed. On the third day, the samples were washed and incubated with a biotin solution. Subsequently, the samples were incubated with a Streptavidin Alexa Fluor® 568 conjugate. For mounting, the samples followed the same procedure as described. The detailed protocol can be found in Appendix D.

The co-localization between Sca-1 and lumican was detected in the bone marrow. This staining procedure resulted in areas with positive co-localization. All of the lumican signaling co-localized with positive Sca-1 signaling. Only a select portion of Sca-1 positive cells were also positive for lumican expression. Co-localization is represented by an orange color (Figure 4.4). The areas of lumican stain are represented by the color red. A green color was used to identify the areas in which Sca-1 was observed (Figure 4.4). The 5-month-old DIO group was used as the trial sample for this procedure. For further research, this staining experiment will be conducted on the remaining 5-month-old samples for each diet group. Analysis will allow for the determination of the percentage of area that is positive for both lumican and Sca-1. This will indicate the amount of MSCs that are correlated with lumican expression.

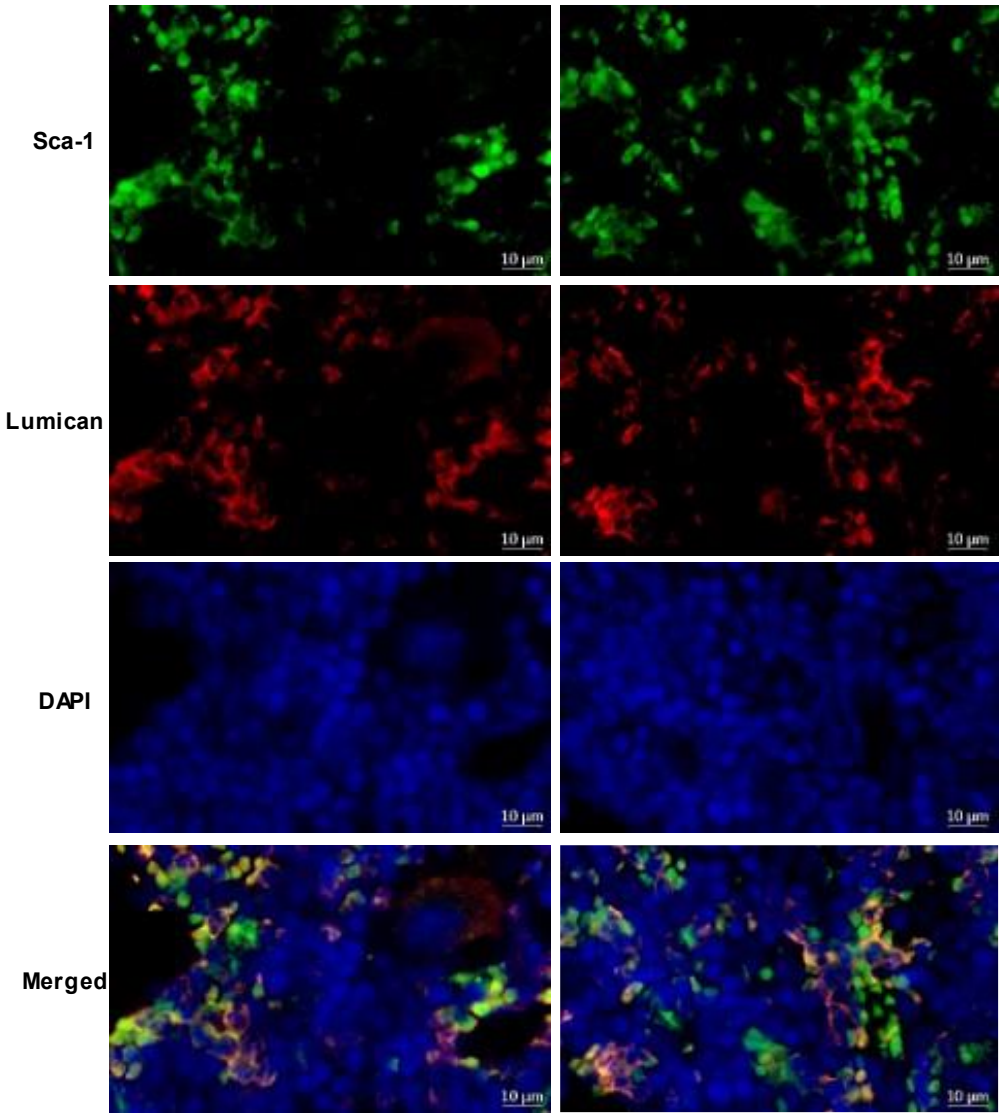

Figure 4.4: IF images from the lumican-Sca-1 co-stain of the bone marrow of a 5-month-old DIO sample. Sca-1 (green) imaged at 647nm, lumican (red) at 568nm, and DAPI (blue) at 360nm. Areas of orange color indicate co-localization of lumican and Sca-1, n=1.

Further verification and analysis will be achieved through an increase in sample size for each group.

Conclusion and discussion

Cells of the stromal fraction that are negative for CD45 antigen express lumican. As determined by IF-staining, the cells that were lumican positive correlated with Sca-1 positive signal. However, not all of the Sca-1 signal was co-localized with lumican signal.

Being able to isolate which cells are associated with lumican expression would lead to the function of lumican in the bone marrow. Through IF-staining, some cells that expressed the MSC marker, Sca-1, were co-localized with lumican expression (Figure 4.4). Of the various cell types that MSCs are able to differentiate into, two of which are osteoblasts and adipocytes.(4) If lumican was expressed by MSCs in a state of obesity, then lumican expression could have influenced a differentiation pathway. An elevated presence of apoptotic cells in the regions of lumican expression does lead to concerns that it is associated with apoptosis. The apoptosis is believed to be caused by the elevated lumican expression. This has been reported previously and experienced through the staining procedure.(52) The exact role of lumican in the bone marrow requires further exploration. *In vitro* experiment of primary MSCs from the bone marrow in the presence of recombinant lumican may allow observations as to allude to the true nature of lumican in the bone marrow. With the utilization of MSCs *in vitro,* we will be able to assess if recombinant lumican can cause apoptosis of MSCs or assist in specific differentiation pathways.

Summary

Apoptotic cells were found to be correlated with regions that had elevated lumican expression in DIO mice. Further confirmation of how lumican expression is associated with apoptosis is still needed. Isolation of stromal cells within the bone marrow led to the determination that lumican was primarily expressed by cells within the bone marrow stromal fraction. IF-staining can allow the visualization of cells that expressed both lumican and Sca-1. Analysis and verification of co-localization will be needed to confirm if lumican is expressed by only a portion of Sca-1 positive cells. Further experiments will be required to explore which stromal cells express lumican. It will also be of interest to determine the effect lumican expression has on cellular fate of MSCs.

Chapter 5: Limitations of Our Study and Future Directions

The biggest limitation of the study was the accessibility to the research facility as a student during COVID-19 restrictions. Any experiments completed could have been conducted at an earlier time to allow for further research in related directions. Regardless, we were able to continue the project to investigate the influence of obesity on bone as well as presence of lumican in the bone marrow of mice.

Immunofluorescence allowed the visualization of the locations for lumican and other primary antibodies within the distal femur. The quantitative analysis for the level of antibody expression may not be the most reliable due to the process of imaging. While imaging, the exposure time could be too much and lead to false-positive signals. Decreasing the exposure time can eliminate background signal, but also remove truly positive signals. During analysis, the software used generated a value based on the signal observed in the image. However, the software can inaccurately identify background signal as a positive signal. Immunofluorescent microscopy requires substantial time to correctly adjust signal intensities to represent the image being evaluated.

Initial qPCR results of the trabecular bone indicated that lumican levels were able to be detected. Lumican expression was also found to be elevated in one sample of bone marrow from a DIO mouse. Further experimentation would be needed to confirm this specific finding. The qPCR and co-staining of lumican and Sca-1 led the exploration to determine which cells express lumican while the mouse is in a state of obesity. This pursuit would require the ability to isolate specific cells of interest from the bone marrow via FACS. RNA would be extracted from these cells to prepare for further experimentation.

To determine the exact cell sub-population that expressed lumican, we were limited on the ability to isolate enough cells for FACS. Using a FACS Aria III sorter, we attempted to gate

for CD45(+) and CD45(-) cells based on their expression of the CD45 antigen. One of the issues resulted in potential cell loss as the cells could only be sorted into 15mL conical tubes. When centrifuging and aspirating the supernatant, cells could have been lost. Combining tubes to attempt to maximize the number of cells per each sub-population may have also resulted in a loss of cells as this is a risk when transferring cells after resuspension. The cellular sorting was designed to be followed by qPCR to confirm which cellular fraction expressed lumican. The experimental plan was to isolate cells positive and negative for a specific antigen. Both sets of cells would have qPCR analysis done on them to determine lumican expression. The goal will be to isolate the MSCs within the bone marrow by sorting for all CD45(-), CD31(-), Sca-1(+), and CD140a(+) cells and determine the level of lumican expression.

To evaluate the role of lumican expression on bone marrow MSCs *in vitro*, these cells are currently being cultured. Unlike other stem cells, these cells appear to have difficulty growing by having a slow growth rate. Once the cell population is usable, the cells will be exposed to recombinant lumican with varying concentrations. We will expose the cells to 0.1µg/mL, 0.2µg/mL and 0.5µg/mL to determine how different concentrations impact the cellular fates. From there we will see what effect lumican has on osteogenic and adipogenic differentiation by induction of these cellular pathways and at what level apoptosis will occur in MSCs. If adipogenic differentiation is more prevalent, then lumican may associated with the replacement of bone cells with adipocytes.

When mice are in a prolonged state of obesity, there are cellular mechanisms activated that result in altered bone homeostasis. Results from µCT imaging indicated that obese mice had significant changes in the trabecular structure and formation. Further investigation into the distal femur led to the finding that a small, leucine-rich proteoglycan, lumican, was substantially more

elevated in DIO bone samples. While lumican has been reported to be present in the trabecular bone cells, we were able to detect its presence in the bone marrow. To determine the role that lumican has in the bone marrow during an obese state, more experimentation is needed. When specific cells from the bone marrow are isolated, it would be possible to monitor the cellular differentiation pathways in varying conditions. In doing so, the role of lumican has on bone homeostasis could be further evaluated.

References

1. Chooi YC, Ding C, Magkos F. The epidemiology of obesity. Metabolism. 2019;92:6-10. Epub 2018/09/27. doi: 10.1016/j.metabol.2018.09.005. PubMed PMID: 30253139.
2. Martyn JA, Kaneki M, Yasuhara S. Obesity-induced insulin resistance and hyperglycemia: etiologic factors and molecular mechanisms. Anesthesiology. 2008;109(1):137-48. Epub 2008/06/27. doi: 10.1097/ALN.0b013e3181799d45. PubMed PMID: 18580184; PMCID: PMC3896971.
3. Wild S, Roglic G, Green A, Sicree R, King H. Global prevalence of diabetes: estimates for the year 2000 and projections for 2030. Diabetes Care. 2004;27(5):1047-53. Epub 2004/04/28. doi: 10.2337/diacare.27.5.1047. PubMed PMID: 15111519.
4. Cao JJ. Effects of obesity on bone metabolism. J Orthop Surg Res. 2011;6:30. Epub 2011/06/17. doi: 10.1186/1749-799X-6-30. PubMed PMID: 21676245; PMCID: PMC3141563.
5. Murray CE, Coleman CM. Impact of Diabetes Mellitus on Bone Health. Int J Mol Sci. 2019;20(19). Epub 2019/10/03. doi: 10.3390/ijms20194873. PubMed PMID: 31575077; PMCID: PMC6801685.
6. Cao JJ, Sun L, Gao H. Diet-induced obesity alters bone remodeling leading to decreased femoral trabecular bone mass in mice. Ann N Y Acad Sci. 2010;1192:292-7. Epub 2010/04/16. doi: 10.1111/j.1749-6632.2009.05252.x. PubMed PMID: 20392249.
7. Fujita Y, Maki K. High-fat diet-induced obesity triggers alveolar bone loss and spontaneous periodontal disease in growing mice. BMC Obes. 2015;3:1. Epub 2016/01/23. doi: 10.1186/s40608-016-0082-8. PubMed PMID: 26793316; PMCID: PMC4705635.
8. Patel VS, Ete Chan M, Rubin J, Rubin CT. Marrow Adiposity and Hematopoiesis in Aging and Obesity: Exercise as an Intervention. Curr Osteoporos Rep. 2018;16(2):105-15. Epub 2018/02/25. doi: 10.1007/s11914-018-0424-1. PubMed PMID: 29476393; PMCID: PMC5866776.
9. Konnecke I, Serra A, El Khassawna T, Schlundt C, Schell H, Hauser A, Ellinghaus A, Volk HD, Radbruch A, Duda GN, Schmidt-Bleek K. T and B cells participate in bone repair by infiltrating the fracture callus in a two-wave fashion. Bone. 2014;64:155-65. Epub 2014/04/12. doi: 10.1016/j.bone.2014.03.052. PubMed PMID: 24721700.
10. Rolighed L, Rejnmark L, Christiansen P. Bone Involvement in Primary Hyperparathyroidism and Changes After Parathyroidectomy. Eur Endocrinol. 2014;10(1):84-7. Epub 2014/02/01. doi: 10.17925/EE.2014.10.01.84. PubMed PMID: 29872470; PMCID: PMC5983103.
11. Fairfield H, Falank C, Harris E, Demambro V, McDonald M, Pettitt JA, Mohanty ST, Croucher P, Kramer I, Kneissel M, Rosen CJ, Reagan MR. The skeletal cell-derived molecule sclerostin drives bone marrow adipogenesis. J Cell Physiol. 2018;233(2):1156-67. Epub 2017/05/02. doi: 10.1002/jcp.25976. PubMed PMID: 28460416; PMCID: PMC5664178.
12. Greco EA, Lenzi A, Migliaccio S. The obesity of bone. Ther Adv Endocrinol Metab. 2015;6(6):273-86. Epub 2015/12/02. doi: 10.1177/2042018815611004. PubMed PMID: 26623005; PMCID: PMC4647134.
13. Evans AL, Paggiosi MA, Eastell R, Walsh JS. Bone density, microstructure and strength in obese and normal weight men and women in younger and older adulthood. J Bone Miner Res. 2015;30(5):920-8. Epub 2014/11/18. doi: 10.1002/jbmr.2407. PubMed PMID: 25400253.
14. Sornay-Rendu E, Boutroy S, Vilayphiou N, Claustrat B, Chapurlat RD. In obese postmenopausal women, bone microarchitecture and strength are not commensurate to greater body weight: the Os des Femmes de Lyon (OFELY) study. J Bone Miner Res. 2013;28(7):1679-87. Epub 2013/02/02. doi: 10.1002/jbmr.1880. PubMed PMID: 23371055.
15. Drel VR, Mashtalir N, Ilnytska O, Shin J, Li F, Lyzogubov VV, Obrosova IG. The leptin-deficient (ob/ob) mouse: a new animal model of peripheral neuropathy of type 2 diabetes and obesity. Diabetes. 2006;55(12):3335-43. Epub 2006/11/30. doi: 10.2337/db06-0885. PubMed PMID: 17130477.

16. Nilsson C, Raun K, Yan FF, Larsen MO, Tang-Christensen M. Laboratory animals as surrogate models of human obesity. Acta Pharmacol Sin. 2012;33(2):173-81. Epub 2012/02/04. doi: 10.1038/aps.2011.203. PubMed PMID: 22301857; PMCID: PMC4010334.
17. Ahima RS. Revisiting leptin's role in obesity and weight loss. J Clin Invest. 2008;118(7):2380-3. Epub 2008/06/24. doi: 10.1172/JCI36284. PubMed PMID: 18568083; PMCID: PMC2430504.
18. Lang P, Hasselwander S, Li H, Xia N. Effects of different diets used in diet-induced obesity models on insulin resistance and vascular dysfunction in C57BL/6 mice. Sci Rep. 2019;9(1):19556. Epub 2019/12/22. doi: 10.1038/s41598-019-55987-x. PubMed PMID: 31862918; PMCID: PMC6925252.
19. Fujita Y, Watanabe K, Maki K. Serum leptin levels negatively correlate with trabecular bone mineral density in high-fat diet-induced obesity mice. J Musculoskelet Neuronal Interact. 2012;12(2):84-94. Epub 2012/06/01. PubMed PMID: 22647282.
20. Devlin MJ, Robbins A, Cosman MN, Moursi CA, Cloutier AM, Louis L, Van Vliet M, Conlon C, Bouxsein ML. Differential effects of high fat diet and diet-induced obesity on skeletal acquisition in female C57BL/6J vs. FVB/NJ Mice. Bone Rep. 2018;8:204-14. Epub 2018/06/30. doi: 10.1016/j.bonr.2018.04.003. PubMed PMID: 29955639; PMCID: PMC6020275.
21. Cao JJ, Gregoire BR, Gao H. High-fat diet decreases cancellous bone mass but has no effect on cortical bone mass in the tibia in mice. Bone. 2009;44(6):1097-104. Epub 2009/03/07. doi: 10.1016/j.bone.2009.02.017. PubMed PMID: 19264159.
22. Patsch JM, Kiefer FW, Varga P, Pail P, Rauner M, Stupphann D, Resch H, Moser D, Zysset PK, Stulnig TM, Pietschmann P. Increased bone resorption and impaired bone microarchitecture in short-term and extended high-fat diet-induced obesity. Metabolism. 2011;60(2):243-9. Epub 2010/02/23. doi: 10.1016/j.metabol.2009.11.023. PubMed PMID: 20171704; PMCID: PMC6342255.
23. Manolagas SC. From estrogen-centric to aging and oxidative stress: a revised perspective of the pathogenesis of osteoporosis. Endocr Rev. 2010;31(3):266-300. Epub 2010/01/07. doi: 10.1210/er.2009-0024. PubMed PMID: 20051526; PMCID: PMC3365845.
24. Dong XN, Qin A, Xu J, Wang X. In situ accumulation of advanced glycation endproducts (AGEs) in bone matrix and its correlation with osteoclastic bone resorption. Bone. 2011;49(2):174-83. Epub 2011/05/03. doi: 10.1016/j.bone.2011.04.009. PubMed PMID: 21530698; PMCID: PMC3117937.
25. Vashishth D, Gibson GJ, Khoury JI, Schaffler MB, Kimura J, Fyhrie DP. Influence of nonenzymatic glycation on biomechanical properties of cortical bone. Bone. 2001;28(2):195-201. Epub 2001/02/22. doi: 10.1016/s8756-3282(00)00434-8. PubMed PMID: 11182378.
26. Mostaco-Guidolin L, Rosin NL, Hackett TL. Imaging Collagen in Scar Tissue: Developments in Second Harmonic Generation Microscopy for Biomedical Applications. Int J Mol Sci. 2017;18(8). Epub 2017/08/16. doi: 10.3390/ijms18081772. PubMed PMID: 28809791; PMCID: PMC5578161.
27. Williams RM, Zipfel WR, Webb WW. Interpreting second-harmonic generation images of collagen I fibrils. Biophysical journal. 2005;88(2):1377-86. Epub 2004/11/08. doi: 10.1529/biophysj.104.047308. PubMed PMID: 15533922.
28. Abraham T, Kayra D, McManus B, Scott A. Quantitative assessment of forward and backward second harmonic three dimensional images of collagen Type I matrix remodeling in a stimulated cellular environment. J Struct Biol. 2012;180(1):17-25. Epub 2012/05/23. doi: 10.1016/j.jsb.2012.05.004. PubMed PMID: 22609365; PMCID: PMC4858383.
29. Kao WW, Funderburgh JL, Xia Y, Liu CY, Conrad GW. Focus on molecules: lumican. Exp Eye Res. 2006;82(1):3-4. Epub 2005/10/11. doi: 10.1016/j.exer.2005.08.012. PubMed PMID: 16213485; PMCID: PMC2876311.
30. Amjadi S, Mai K, McCluskey P, Wakefield D. The role of lumican in ocular disease. ISRN Ophthalmol. 2013;2013:632302. Epub 2014/02/22. doi: 10.1155/2013/632302. PubMed PMID: 24558602; PMCID: PMC3914189.

31. Kao WW, Liu CY. Roles of lumican and keratocan on corneal transparency. Glycoconj J. 2002;19(4-5):275-85. Epub 2003/09/17. doi: 10.1023/A:1025396316169. PubMed PMID: 12975606.
32. Peyrin F, Dong P, Pacureanu A, Langer M. Micro- and nano-CT for the study of bone ultrastructure. Curr Osteoporos Rep. 2014;12(4):465-74. Epub 2014/10/09. doi: 10.1007/s11914-014-0233-0. PubMed PMID: 25292366.
33. Bouxsein ML, Boyd SK, Christiansen BA, Guldberg RE, Jepsen KJ, Muller R. Guidelines for assessment of bone microstructure in rodents using micro-computed tomography. J Bone Miner Res. 2010;25(7):1468-86. Epub 2010/06/10. doi: 10.1002/jbmr.141. PubMed PMID: 20533309.
34. Glatt V, Canalis E, Stadmeyer L, Bouxsein ML. Age-related changes in trabecular architecture differ in female and male C57BL/6J mice. J Bone Miner Res. 2007;22(8):1197-207. Epub 2007/05/10. doi: 10.1359/jbmr.070507. PubMed PMID: 17488199.
35. Shapses SA, Sukumar D. Bone metabolism in obesity and weight loss. Annu Rev Nutr. 2012;32:287-309. Epub 2012/07/20. doi: 10.1146/annurev.nutr.012809.104655. PubMed PMID: 22809104; PMCID: PMC4016236.
36. Aguiari P, Leo S, Zavan B, Vindigni V, Rimessi A, Bianchi K, Franzin C, Cortivo R, Rossato M, Vettor R, Abatangelo G, Pozzan T, Pinton P, Rizzuto R. High glucose induces adipogenic differentiation of muscle-derived stem cells. Proc Natl Acad Sci U S A. 2008;105(4):1226-31. Epub 2008/01/24. doi: 10.1073/pnas.0711402105. PubMed PMID: 18212116; PMCID: PMC2234120.
37. Jacobs CR. The mechanobiology of cancellous bone structural adaptation. J Rehabil Res Dev. 2000;37(2):209-16. Epub 2000/06/13. PubMed PMID: 10850827.
38. Khajuria DK, Soliman M, Elfar JC, Lewis GS, Abraham T, Kamal F, Elbarbary RA. Aberrant structure of fibrillar collagen and elevated levels of advanced glycation end products typify delayed fracture healing in the diet-induced obesity mouse model. Bone. 2020;137:115436. Epub 2020/05/23. doi: 10.1016/j.bone.2020.115436. PubMed PMID: 32439570.
39. Abraham T, Clawson G, Linton S, McGovern C, Tang X, Adair J, Matters G. Bio-distribution of near infrared imaging agent loaded targeted drug nanoparticle carriers in highly fibrotic pancreatic tumor determined using multiphoton and harmonic generation imaging: SPIE; 2018.
40. Abraham T, Hogg J. Extracellular matrix remodeling of lung alveolar walls in three dimensional space identified using second harmonic generation and multiphoton excitation fluorescence. J Struct Biol. 2010;171(2):189-96. Epub 2010/04/24. doi: 10.1016/j.jsb.2010.04.006. PubMed PMID: 20412859.
41. Feng X. Chemical and Biochemical Basis of Cell-Bone Matrix Interaction in Health and Disease. Curr Chem Biol. 2009;3(2):189-96. Epub 2010/02/18. doi: 10.2174/187231309788166398. PubMed PMID: 20161446; PMCID: PMC2790195.
42. Viguet-Carrin S, Garnero P, Delmas PD. The role of collagen in bone strength. Osteoporos Int. 2006;17(3):319-36. Epub 2005/12/13. doi: 10.1007/s00198-005-2035-9. PubMed PMID: 16341622.
43. Alzamil H. Elevated Serum TNF-alpha Is Related to Obesity in Type 2 Diabetes Mellitus and Is Associated with Glycemic Control and Insulin Resistance. J Obes. 2020;2020:5076858. Epub 2020/02/25. doi: 10.1155/2020/5076858. PubMed PMID: 32089876; PMCID: PMC7013317 publication of this paper.
44. Zhang H, Recker R, Lee WN, Xiao GG. Proteomics in bone research. Expert Rev Proteomics. 2010;7(1):103-11. Epub 2010/02/04. doi: 10.1586/epr.09.90. PubMed PMID: 20121480; PMCID: PMC2848984.
45. Nesvizhskii AI, Keller A, Kolker E, Aebersold R. A statistical model for identifying proteins by tandem mass spectrometry. Anal Chem. 2003;75(17):4646-58. Epub 2003/11/25. doi: 10.1021/ac0341261. PubMed PMID: 14632076.
46. Shadforth IP, Dunkley TP, Lilley KS, Bessant C. i-Tracker: for quantitative proteomics using iTRAQ. BMC Genomics. 2005;6:145. Epub 2005/10/26. doi: 10.1186/1471-2164-6-145. PubMed PMID: 16242023; PMCID: PMC1276793.

47. Oberg AL, Mahoney DW, Eckel-Passow JE, Malone CJ, Wolfinger RD, Hill EG, Cooper LT, Onuma OK, Spiro C, Therneau TM, Bergen HR, 3rd. Statistical analysis of relative labeled mass spectrometry data from complex samples using ANOVA. J Proteome Res. 2008;7(1):225-33. Epub 2008/01/05. doi: 10.1021/pr700734f. PubMed PMID: 18173221; PMCID: PMC2528956.
48. Raouf A, Ganss, B, McMahon, C, Vary, C, Roughley, P. J, Seth, A. Lumican is a major proteoglycan component of the bone matrix. Matrix Biology. 2002;21(4):361-7. doi: 10.1016/s0945-053x(02)00027-6; PMCID: 12128073.
49. Hsiao KC, Chu PY, Chang GC, Liu KJ. Elevated Expression of Lumican in Lung Cancer Cells Promotes Bone Metastasis through an Autocrine Regulatory Mechanism. Cancers (Basel). 2020;12(1). Epub 2020/01/23. doi: 10.3390/cancers12010233. PubMed PMID: 31963522; PMCID: PMC7016828.
50. Mohamed AM. An overview of bone cells and their regulating factors of differentiation. Malays J Med Sci. 2008;15(1):4-12. Epub 2008/01/01. PubMed PMID: 22589609; PMCID: PMC3341892.
51. Vij N, Roberts L, Joyce S, Chakravarti S. Lumican suppresses cell proliferation and aids Fas-Fas ligand mediated apoptosis: implications in the cornea. Exp Eye Res. 2004;78(5):957-71. Epub 2004/03/31. doi: 10.1016/j.exer.2003.12.006. PubMed PMID: 15051477.
52. Williams KE, Fulford LA, Albig AR. Lumican reduces tumor growth via induction of fas-mediated endothelial cell apoptosis. Cancer Microenviron. 2010;4(1):115-26. Epub 2010/01/01. doi: 10.1007/s12307-010-0056-1. PubMed PMID: 21505566; PMCID: PMC3047633.
53. Yamada A, Arakaki R, Saito M, Kudo Y, Ishimaru N. Dual Role of Fas/FasL-Mediated Signal in Peripheral Immune Tolerance. Front Immunol. 2017;8:403. Epub 2017/04/21. doi: 10.3389/fimmu.2017.00403. PubMed PMID: 28424702; PMCID: PMC5380675.
54. Kyrylkova K, Kyryachenko S, Leid M, Kioussi C. Detection of apoptosis by TUNEL assay. Methods Mol Biol. 2012;887:41-7. Epub 2012/05/09. doi: 10.1007/978-1-61779-860-3_5. PubMed PMID: 22566045.
55. Holmes C, Stanford WL. Concise review: stem cell antigen-1: expression, function, and enigma. Stem Cells. 2007;25(6):1339-47. Epub 2007/03/24. doi: 10.1634/stemcells.2006-0644. PubMed PMID: 17379763.

Appendix

Appendix A: Detailed Protocol of the TNF-α immunofluorescent staining procedure

DAY:1

Deparaffinization:

1- 3x5 minutes in Xylene
2- 2x5 minutes in 100% Ethanol
3- 2x5 minutes in 95% Ethanol
4- 1x2 minutes in 70% Ethanol
5- 2x1minute in Deionized Water
6- Place slides in 1X TBS for short term storage until antigen retrieval step.

Antigen Retrieval:

1- Make a 0.5% Pepsin/HCl solution.
2- Combine 200mL of DI H_2O and 1.0g of Pepsin, stir until dissolved.
3- Add 2mL of 0.5N HCl to lower the pH, activating the pepsin.
4- Warm the solution for 30 minutes at 37°C to allow the solution for optimal temperature.
5- Submerse slides in the 0.5% Pepsin/HCl solution for 10 minutes at 37°C.

Permeabilization:

1- Place slides in 0.03% TritonX TBS for 30 minutes.
2- Submerse slides two times in 1X TBS for 5 minutes each.

Blocking:

1- Using a hydrophobic pen/marker, draw a circle around the sample.
2- Apply 100µL of 10% Normal Goat Serum (NGS) to cover the entire sample.
3- Incubate at RT for 2 hours.
4- Do not wash.

Primary Antibody: Anti-TNF alpha antibody (ab9739)

1- Make a 1% NGS, 1% Primary Antibody solution in 1X TBS.
2- Apply 100µL to cover each sample and incubate overnight at 4°C.

DAY:2

Steptavidin Alexa Fluor® 647 Conjugate

1- Make a 1% NGS, 1% Biotin (Rabbit-Goat) in 1X TBS.
2- Apply 100µL Biotin solution to each sample, incubate at RT for 1 hour.
3- Wash samples in 1X TBS, 3x5 minutes.
4- Make a 1% NGS, 1% Streptavidin AF647 solution in 1X TBS.
5- Apply 100µL to cover each sample, incubate in the DARK at RT for 1 hour.

*Limit exposure to light from this point forward.

6- Wash in 1X TBS 3x5 minutes.
7- Soak in 0.03% Triton X in TBS for 5 minutes.

8- Wash two more times in 1X TBS for 5 minutes each.

Mounting:

1- Remove excess liquid from slide, keeping careful attention not to touch the sample.
2- Apply one drop of DAPI Pro-long Gold Mounting Media.
3- Place coverslip gently at an angle to allow the mounting media to spread evenly, avoiding air bubbles.
4- After slides have dried, apply clear nail polish to edges of cover slip to seal the edges.
5- Store slides at 4°C to preserve signal.

Appendix B: Detailed Protocol of the Lumican immunofluorescent staining procedure

DAY: 1

Deparaffinization:

1- 3x5 minutes in Xylene
2- 2x5 minutes in 100% Ethanol
3- 2x5 minutes in 95% Ethanol
4- 1x2 minutes in 70% Ethanol
5- 2x1minute in Deionized Water
6- Place slides in 1X TBS for short term storage until antigen retrieval step.

Antigen Retrieval:

1- Make a 0.5% Pepsin/HCl solution.
2- Combine 200mL of DI H_2O and 1.0g of Pepsin, stir until dissolved.
3- Add 2mL of 0.5N HCl to lower the pH, activating the pepsin.
4- Warm the solution for 30 minutes at 37°C to allow the solution for optimal temperature.
5- Submerse slides in the 0.5% Pepsin/HCl solution for 30 minutes at 37°C.

Permeabilization:

1- Place slides in 0.03% TritonX TBS for 30 minutes.
2- Submerse slides two times in 1X TBS for 5 minutes each.

Blocking:

1- Using a hydrophobic pen/marker, draw a circle around the sample.
2- Apply 100µL of 10% Normal Goat Serum (NGS) to cover the entire sample.
3- Incubate at RT for 2 hours.
4- Do not wash.

Primary Antibody: Lumican - ab168348 Rb to mAb to Lumican [EPR8898(2)]

1- Make a 1% NGS, 1% Primary Antibody solution in TBS.
2- Apply 100µL to cover each sample and incubate overnight at 4°C.

DAY:2

Steptavidin Alexa Fluor® 647 Conjugate

1- Biotin solution to increase strength of streptavidin adherence.
2- Make a 1% NGS, 1% Biotin (Rabbit-Goat) in 1X TBS.
3- Apply 100µL Biotin solution to each sample, incubate at RT for 1 hour.
4- Wash samples in 1X TBS, 3x5 minutes.
5- Make a 1% NGS, 1% Streptavidin AF647 solution in 1X TBS.
6- Apply 100µL to cover each sample, incubate in the DARK at RT for 1 hour.

*Limit exposure to light from this point forward.

7- Wash in 1X TBS 3x5 minutes.
8- Soak in 0.03% Triton X in TBS for 5 minutes.
9- Wash two more times in 1X TBS for 5 minutes each.

Mounting:

1- Remove excess liquid from slide, keeping careful attention not to touch the sample.
2- Apply one drop of DAPI Pro-long Gold Mounting Media.
3- Place coverslip gently at an angle to allow the mounting media to spread evenly, avoiding air bubbles.
4- After slides have dried, apply clear nail polish to edges of cover slip to seal the edges.
5- Store slides at 4°C to preserve signal.

Appendix C: Detailed Staining Procedure for TUNEL Assay

Preparation for first time:

1- Make 1X Click-IT® Plus TUNEL Reaction Buffer
    a. Transfer the 10X concentrate to 4.5mL of DH_2O.
2- Make a 1X Click-IT® Plus TUNEL Supermix by combining:
    a. 2625µL of 1X Click-IT® Plus TUNEL Reaction Buffer
    b. 67µL of Copper Protectant
    c. 8.3µL of Picolyl Azide Alexa Fluor® 647
3- Make a 100X stock solution of Click-IT® Plus TUNEL Reaction Buffer Additive by adding 2mL of DH_2O to the 400mg of additive.
4- Make a 1X Proteinase K solution by diluting the stock to 1:25 with 1X TBS.

Deparaffinization:

1- 3x5 minutes in Xylene
2- 2x5 minutes in 100% Ethanol
3- 2x5 minutes in 95% Ethanol
4- 1x2 minutes in 70% Ethanol
5- 2x1minute in Deionized Water
6- Place slides in 1X TBS for short term storage.

Fixation and Permeabilization:

1- Apply 100µL of 4% Paraformaldehyde (PFA) for 15 minutes at 37°C ensuring that specimen is covered.
2- Wash slides in 1X TBS for 2x5 minutes.
3- Apply 70µL of the Proteinase K solution, covering the entire specimen.
    a. Place slides in a humidified camber for 15 minutes at RT.
4- Wash slides in 1X TBS for 5 minutes
5- Apply 100µL of 4% PFA, covering the entire sample, for 5 minutes at 37°C.
6- Wash slides in 1X TBS for 2x5 minutes
7- Rinse slides with DH_2O

TdT Reaction:

1- Cover the samples with 100µL of TdT Reaction Buffer for 10 minutes at 37°C.
2- Prepare TdT reaction mixture based on number of slides, with each slide having:
    a. 47µL of TdT reaction buffer
    b. 1µL of EdUTP
    c. 2µL of TdT enzyme
3- After removing TdT buffer from slides, add 50µL of TdT reaction mixture to each sample for 60 minutes at 37°C, placing the slides within a humidified chamber.
4- Rinse slides with DH_2O.
5- Wash slides in 3% BSA and 0.1% Triton® X-100 in 1X TBS for 5 minutes.
6- Submerge slides in 1X TBS for 5 minutes.

Click-IT® Plus Reaction

1- Prepare an aliquot of 10X Click-IT® Plus TUNEL Buffer additive by diluting the 100X stock solution with DH_2O.
2- Prepare a Click-IT® Plus TUNEL Reaction cocktail within 15 minutes for each slide:
    a. 45µL of Click-IT® Plus TUNEL Supermix
    b. 5µL of 10X Click-IT® Plus Reaction buffer additive
    c. Incubate at 37°C for 30 minutes protecting from light.

*Protect from light from this point forward.

3- Remove the reaction cocktail and wash slides in 3% BSA in 1X TBS for 5 minutes.
4- Rinse slides in 1X TBS for 5 minutes.

Mounting:

1- Remove excess liquid from slide, keeping careful attention not to touch the sample.
2- Apply one drop of DAPI Pro-long Gold Mounting Media.
3- Place coverslip gently at an angle to allow the mounting media to spread evenly, avoiding air bubbles.
4- After slides have dried, apply clear nail polish to edges of cover slip to seal the edges.
5- Store slides at 4°C to preserve signal.

Appendix D: Detailed Staining Procedure for Lumican and SCA-1 Co-stain

DAY:1

Deparaffinization:

1- 3x5 min. Xylene
2- 2x5 min. 100% EtOH
3- 2x5 min. 95% EtOH
4- 1x2 min. 70% EtOH
5- 2x1 min. DH_20
6- Place in 1X TBS for short-term storage or until Antigen retrieval.

Antigen Retrieval:

1- Make a 0.5% Pepsin/HCl solution.
2- Combine 200mL of DI H_2O and 1.0g of Pepsin, stir until dissolved.
3- Add 2mL of 0.5N HCl to lower the pH, activating the pepsin.
4- Warm the solution for 30 minutes at 37°C to allow the solution for optimal temperature.
5- Submerse slides in the 0.5% Pepsin/HCl solution for 20 minutes at 37°C.

Blocking:

1- Using a hydrophobic pen/marker, draw a circle around the sample.
2- Apply 100µL of 10% Normal Goat Serum (NGS) to cover the entire sample.
3- Incubate at RT for 2 hours.
4- Do not wash.

Primary Antibody: Alexa Fluor® 647 anti-mouse Ly-6A/E (Sca-1), Clone: D7, Cat: 108118

1- Make a 1% NGS, 1% Primary Antibody solution in TBS.
2- Apply 100µL to cover each sample and incubate overnight at 4°C.

*Limit exposure to light from this point forward

DAY 2

Primary Antibody #2: Lumican - ab168348 Rb to mAb to Lumican [EPR8898(2)]

1- Wash 3x in 1X TBS for 5 min. each
2- Make 1% NGS, 1% Lumican with 1X TBS.
    a. Ex: (1µL NGS, 1µL primary, 98µL 1X TBS to make 1:100)
3- Apply 100µL to each sample.
4- Incubate at 4ºC overnight.

DAY 3:

Streptavidin Alexa Fluor® 568 Conjugate

1- Biotin solution to increase strength of streptavidin adherence.
2- Make a 1% NGS, 1% Biotin (Rabbit-Goat) in 1X TBS.
3- Apply 100µL Biotin solution to each sample, incubate at RT for 1 hour.
4- Wash samples in 1X TBS, 3x5 minutes.
5- Make a 1% NGS, 1% Streptavidin AF568 solution in 1X TBS.

6- Apply 100µL to cover each sample, incubate in the DARK at RT for 1 hour.

*Limit exposure to light from this point forward.

7- Wash in 1X TBS 3x5 minutes.
8- Wash two more times in 1X TBS for 5 minutes each.

Mounting:

1- Remove excess liquid from slide, keeping careful attention not to touch the sample.
2- Apply one drop of DAPI Pro-long Gold Mounting Media.
3- Place coverslip gently at an angle to allow the mounting media to spread evenly, avoiding air bubbles.
4- After slides have dried, apply clear nail polish to edges of cover slip to seal the edges.
5- Store slides at 4°C to preserve signal.

Appendix E: RNA Extraction Results of Distal Femur Trabecular Bone Tissue

Sample #	Age (Months)	Diet	[RNA] ng/µL	A260/280	A260/230
38	5	Lean	1288.223	1.879	1.969
39	5	Lean	2401.684	1.880	2.153
42	5	Lean	1745.869	1.874	2.184
44	5	Lean	1899.300	1.890	2.180
46	5	Lean	887.700	1.870	2.040
30	5	DIO	1241.083	1.857	1.231
33	5	DIO	1020.202	1.841	1.638
36	5	DIO	1584.952	1.870	2.124
35	5	DIO	1466.325	1.865	2.100
25	5	DIO	1562.500	1.840	2.090
20	8	Lean	1850.500	1.880	2.170
21	8	Lean	1991.100	1.880	2.190
11	8	Lean	1854.000	1.820	2.080
12	8	Lean	2154.900	1.870	2.100
24	8	DIO	1404.900	1.890	2.050
16	8	DIO	1232.800	1.830	2.160
23	8	DIO	1936.500	1.850	2.110
5	8	DIO	1690.900	1.860	2.160

Appendix F: Quantitative Proteomic Analysis Results

Identified Proteins (1589/1602)	Accession Number	Molecular Weight (kDa)	Log2 Fold Change (DIO /lean)
Upregulated			
lumican precursor [Mus musculus]	NP_032550.2	38	7.82
protein S100-A10 [Mus musculus]	NP_033138.1 (+1)	11	5.62
catalase [Mus musculus]	NP_033934.2	60	5.59
predicted gene 4737 [Mus musculus]	NP_001291457.1 (+1)	48	4.64
ubiquitin carboxyl-terminal hydrolase isozyme L3 [Mus musculus]	NP_057932.2 (+3)	26	4.6
glutathione hydrolase 5 proenzyme isoform 1 precursor [Mus musculus]	NP_035950.2	62	4.45
heat shock protein 105 kDa isoform 2 [Mus musculus]	NP_001334463.1 (+3)	92	4.37
phosphoribosyl pyrophosphate synthase-associated protein 1 [Mus musculus]	NP_080640.1 (+1)	42	4.3
peroxisomal multifunctional enzyme type 2 [Mus musculus]	NP_032318.2	79	4.28
Cluster of major urinary protein 14 precursor [Mus musculus] (NP_001186928.1)	NP_001186928.1 [4]	21	3.92
Downregulated			
BTB/POZ domain-containing protein KCTD12 [Mus musculus]	NP_808383.3	36	-6.4
eukaryotic translation initiation factor 3 subunit M [Mus musculus]	NP_663355.1	43	-6.3
protein-glutamine gamma-glutamyltransferase 2 [Mus musculus]	NP_033399.1	77	-6.03
P04258 SWISS-PROT:P04258 (Bos taurus) Similar to Collagen alpha 1(III) chain	cont|000279|	138	-6
isocitrate dehydrogenase [NADP] cytoplasmic [Mus musculus]	NP_001104790.1 (+1)	47	-5.89
collagen alpha-1(XI) chain preproprotein [Mus musculus]	NP_031755.2 (+3)	181	-5.22
T-complex protein 1 subunit theta [Mus musculus]	NP_033970.3	60	-5.02
aldehyde dehydrogenase family 3 member B1 [Mus musculus]	NP_080592.2 (+1)	52	-4.95
60S ribosomal protein L24 [Mus musculus]	NP_077180.1	18	-4.9
coiled-coil domain-containing protein 124 [Mus musculus]	NP_081240.1 (+1)	25	-4.7